Progress In Electromagnetics Research, PIER 88, 1–38, 2008

RCS OF LARGE BENT WAVEGUIDE DUCTS FROM A MODAL ANALYSIS COMBINED WITH THE KIRCHHOFF APPROXIMATION

C. Bourlier, H. He, and J. Chauveau

Laboratory IREENA, Polytech'Nantes
Rue Christian Pauc, La Chantrerie
BP 50609, 44306 Nantes Cedex 3, France

R. Hémon and P. Pouliguen

DGA/DET/Centre d'ELectronique de l'ARmement (CELAR)
Bruz 35170, France

Abstract—In this paper, we present a fast method to predict the monostatic Radar Cross Section (RCS) in high-frequency of a cavity, which can be modeled as a succession of bent waveguides of the same cross section and stuffed by a perfectly-conducting termination. Based on a modal analysis combined with the Kirchhoff Approximation, this method allows us to obtain closed-form expressions of the transmission matrix at each discontinuity. In addition, to improve the efficiency, a selective modal scheme is proposed, which selects only the propagating modes contributing to the scattering. Compared to the Iterated Physical Optics (IPO) method and the Multi-Level Fast Multipole Method (MLFMM, generated from the commercial software FEKO), this approach brings good results for cavities with small tilt angles of the bends, typically smaller than 2 degrees.

1. INTRODUCTION

Diffraction from open ended cavities is important in scattering analysis because jet engine inlets are significant contributors to the Radar Cross Section (RCS). This work also finds applications in [1–3] for instance. Anastassiu [4] presented a very interesting review of methods devoted to this challenging task, which can be grouped in three categories: rigorous, asymptotic and hybrid. The reader is invited to read this article for more references. Rigorous methods, based

on the integral equations, can handle arbitrary geometries via an appropriately chosen discretization; but their main limitation is the size of the scatterers. This is why for instance, hybrid boundary-integral/modal approach was developed [5]. In high-frequency, when the cross section of the cavity is large comparatively to the incident wavelength λ_0, asymptotic methods, like approaches based on ray tracing [6–10], Physical Optics [11–14] and modal analysis combined with the Kirchhoff Approximation for the boundary conditions [15–17] are also investigated. This paper applied this latter to an open ended cavity modeled as a succession of bent waveguides of same rectangular cross section and stuffed by a perfectly-conducting termination. From this scheme, a curved cavity can then be treated.

For a two-dimensional waveguide duct containing a bend with a tilt angle of 15 degrees and of $8.7\lambda_0$ height, Ling et al. [18] presented numerical results from this method. By comparing them with the Method of Moments (MoM) [5], a good agreement on the monostatic RCS was obtained for the co-polarizations. Thus, this method should work well for the three-dimensional case. It is one of the purposes of this paper. In addition, unlike [18], closed-form expressions of the elements of the transmission matrix at the bend are derived. Similar works has been done in [19], but in this paper the boundary conditions at the discontinuity are applied rigorously, which then requires to invert a matrix. For canonical terminations, this method referred as to mode matching technique is also employed in [20]. In addition, to accelerate the computation of the sums, we propose a selective modal scheme (similar to the one addressed in [16]), which is applied on each section of the duct waveguide. This fact is especially useful in high-frequency where a direct modal analysis becomes cumbersome and inefficient due to the existence of a large number of propagating modes inside the waveguide cavity region.

The paper is organized as follows. In Section 2, the mathematical formulation is addressed for a waveguide connected to a bent waveguide of same cross section, and in Section 3, the formulation is generalized to a succession of bent waveguides connected between them. In Section 4, our approach is compared with two methods: (i) The Iterated Physical Optics (IPO) one, summarized in [14], which is very appropriate for large cross sections comparatively to the wavelength; (ii) The Multi-Level Fast Multipole Method (MLFMM) one, generated from the commercial software FEKO [21]. In this paper, the multiple-edge diffraction of modal rays across the aperture is assumed to be negligible for a large cross section of the waveguide. As shown in [15], this contribution can be added separately.

2. MATHEMATICAL FORMULATION

In this section, the derivation in the far zone of the scattered field by the cavity presented in Fig. 1 ($N_{\text{wg}} = 1$) is addressed from a modal analysis combined with the Kirchhoff approximation. In Section 4, the formulation is generalized for a cavity composed of N_{wg} bent waveguides with same rectangular cross section.

2.1. Description of the Problem

The problem is presented in Fig. 1. The open ended cavity is modeled as a succession of two waveguides of length $\{L_i\}$ ($i = \{1, 2\}$) and with the same rectangular cross section of area $a \times b$ (a is the dimension along the $\hat{\mathbf{x}}_1$ direction and b the dimension along the $\hat{\mathbf{y}}_1$). The waveguide 2 undergone a rotation of an angle $\theta_{12} = 2\theta_1 = 2\theta_2$ in the plane $(\hat{\mathbf{z}}_1, \hat{\mathbf{y}}_1)$ and its extremity is stuffed by a perfectly-conducting termination. In what follows, the boldface stands for a vector, $\mathbf{u}$, and the hat $\hat{}$ indicates that the vector is unitary ($\hat{\mathbf{u}} = \mathbf{u}/\|\mathbf{u}\|$). The purpose is to derive the diffracted field by such a structure when it is illuminated by a plane wave of direction $\mathbf{k}_i = (k_0 \cos\phi_i \sin\theta_i, k_0 \sin\phi_i \sin\theta_i, k_0 \cos\theta_i) = (k_{ix}, k_{iy}, k_{iz})$. The angles (θ_i, ϕ_i) are depicted in Fig. 1.

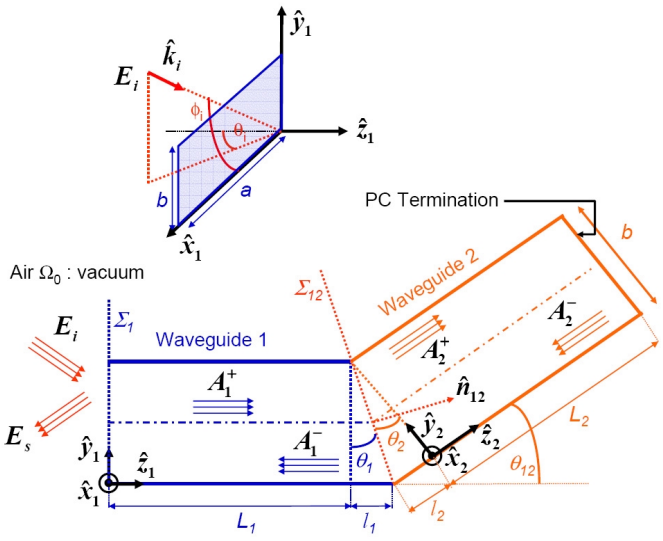

Figure 1. Description of the problem geometry. $l_1 = l_2 = b\tan(\theta_{12}/2)$ and $\theta_{12} = 2\theta_1 = 2\theta_2$.

For a waveguide of canonical cross section and uniform along the $\hat{\mathbf{z}}$ direction, the electromagnetic fields inside the waveguide can be derived analytically by considering two polarizations. The TE case, which means that the electric field $\mathbf{E}$ has no component along the $\hat{\mathbf{z}}_1$ direction. In this paper, the quantities related to this polarization will be marked with the superscript h. The TM case, which means that the magnetic field $\mathbf{H}$ has no component along the $\hat{\mathbf{z}}_1$ direction. In this paper, the quantities related to this polarization will be marked with the superscript e. In addition, for a wave traveling along the positive $\hat{\mathbf{z}}_1$ direction, the superscript $+$ will be used, whereas for a wave traveling along the negative $\hat{\mathbf{z}}_1$ direction, the superscript — will be applied. From [22, 23], in the Cartesian basis $(\hat{\mathbf{x}}, \hat{\mathbf{y}}, \hat{\mathbf{z}})$, we have for the TE case

$$\begin{cases} E_z^{\mp} = 0 \quad H_z^{\mp} = \left(k_c^{\mathrm{h}}\right)^2 e^{\pm j\beta^{\mathrm{h}} z}\psi^{\mathrm{h}} \\ \mathbf{H}_{\mathrm{T}}^{\mp} = \pm j\beta^{\mathrm{h}} e^{\pm j\beta^{\mathrm{h}} z}\boldsymbol{\nabla}_{\mathrm{T}}\psi^{\mathrm{h}} \\ \mathbf{E}_{\mathrm{T}}^{\mp} = j\beta^{\mathrm{h}} Z^{\mathrm{h}} e^{\pm j\beta^{\mathrm{h}} z}\hat{\mathbf{z}} \wedge \boldsymbol{\nabla}_{\mathrm{T}}\psi^{\mathrm{h}} \end{cases}, \tag{1}$$

and for the TM case

$$\begin{cases} H_z^{\mp} = 0 \quad E_z^{\mp} = \left(k_c^{\mathrm{e}}\right)^2 e^{\pm j\beta z}\psi^{\mathrm{e}} \\ \mathbf{E}_{\mathrm{T}}^{\mp} = \pm j\beta^{\mathrm{e}} e^{\pm j\beta^{\mathrm{e}} z}\boldsymbol{\nabla}_{\mathrm{T}}\psi^{\mathrm{e}} \\ \mathbf{H}_{\mathrm{T}}^{\mp} = -j\beta^{\mathrm{e}} Y^{\mathrm{e}} e^{\pm j\beta^{\mathrm{e}} z}\hat{\mathbf{z}} \wedge \boldsymbol{\nabla}_{\mathrm{T}}\psi^{\mathrm{e}} \end{cases}, \tag{2}$$

with $Z^{\mathrm{h}} = \frac{\omega\mu}{\beta}$, $Y^{\mathrm{e}} = \frac{\omega\epsilon}{\beta}$ and $\beta^2 = k_0^2 - k_c^2$ ($k_0 = 2\pi/\lambda_0$). The wavenumber k_c depends on the polarization and on the shape of the cross section. ω is the pulsation, μ is the permeability of the medium Ω inside the waveguide, assumed to be vacuum, and ϵ is the permittivity. The term $e^{\pm j\beta z}$ corresponds to waves propagating in $\mp\hat{\mathbf{z}}$ direction. The symbol $\boldsymbol{\nabla}_{\mathrm{T}}$ is a "del" operator defined in the transverse plane. For instance, $\boldsymbol{\nabla}_{\mathrm{T}} = \frac{\partial}{\partial x}\hat{\mathbf{x}} + \frac{\partial}{\partial y}\hat{\mathbf{y}}$ for a rectangular waveguide. The Cartesian coordinates system (x, y) is then used for the derivations of the eigen functions ψ^{h} and ψ^{e}. For more details, see for instance [22, 23] for the derivations of the functions ψ^{h} and ψ^{e} for canonical cross sections of the waveguide.

The electromagnetic fields inside each waveguide can be derived rigorously from a modal approach given by Eqs. (1) and (2). The aperture of the waveguide 1 and the junction between the waveguides 1 and 2 modified these electromagnetic fields. Via the reciprocity theorem and the boundary conditions, the link between the fields inside the waveguides 1 and 2 and the field radiated by the waveguide 1 can

be computed rigorously by discretizating the integral equations solved, for instance, from the Method of Moments. This operation requires then to invert a matrix, whose its size increases significantly with the wavelength. To overcome this drawback, in this paper the Kirchhoff approximation is applied to determine the boundary conditions at each discontinuity.

The derivation of the scattered fields by the cavity presented in Fig. 1 demands then three steps described in the following subsections:

(i) Electromagnetic fields transmitted into the waveguide 1,

(ii) Reflection matrix of the waveguide 2, which demands three substeps:
   (a) Derivation of the *transmitted* fields into the waveguide 2,
   (b) Derivation of the *reflected* fields onto the waveguide 2,
   (c) Derivation of the *reflected* fields onto the waveguide 1,

(iii) Electromagnetic fields radiated by the waveguide 1.

2.2. First Step — Electromagnetic Fields Transmitted into the Waveguide 1

If the waveguide 1 is illuminated by an incident plane wave, then Eqs. (1) and (2) must be multiplied by A_1^+ (which depends on the polarization, leading to $A_1^{+,\mathrm{h}}$ and $A_1^{+,\mathrm{e}}$) corresponding to the transmission coefficient between the air (medium Ω_0) and the medium Ω. It is derived by applying the boundary conditions on the transverse plane Σ_1 defined at $z = 0$. For a large aperture comparatively to the wavelength λ_0, the boundary conditions can be obtained by applying the Kirchhoff approximation, stating that there are continuities of the electric and magnetic tangential fields. Thus, the surface currents on Σ_1 are $\mathbf{J}_{s0}^+ = \hat{\mathbf{n}}_1 \wedge \mathbf{H}_i = \hat{\mathbf{z}}_1 \wedge \mathbf{H}_i$ (electric) and $\mathbf{M}_{s0}^+ = -\hat{\mathbf{n}}_1 \wedge \mathbf{E}_i = -\hat{\mathbf{z}}_1 \wedge \mathbf{E}_i$ (magnetic), in which $\hat{\mathbf{n}}_1$ is the vector normal to Σ_1 ($\hat{\mathbf{n}}_1 = \hat{\mathbf{z}}_1$). The amplitude A_1^+ can then be found by [23]

$$A_1^{\pm} = -\frac{\displaystyle\int_{\Sigma_1} \left[\left(\mathbf{e}_{\mathrm{T},1}^{\mp} + \mathbf{e}_{z,1}^{\mp} \right) \cdot \mathbf{J}_{s0}^+ - \left(\mathbf{h}_{\mathrm{T},1}^{\mp} + \mathbf{h}_{z,1}^{\mp} \right) \cdot \mathbf{M}_{s0}^+ \right] d\Sigma}{2 \displaystyle\int_{\Sigma_1} \left(\mathbf{e}_{\mathrm{T},1}^{\mp} \wedge \mathbf{h}_{\mathrm{T},1}^{\mp} \right) \cdot \hat{\mathbf{z}}_1 d\Sigma}, \qquad (3)$$

where $\mathbf{e}_1^{\mp} = \mathbf{e}_{\mathrm{T},1}^{\mp} + e_{z,1}^{\mp} \hat{\mathbf{z}}_1$ and $\mathbf{h}_1^{\mp} = \mathbf{h}_{\mathrm{T},1}^{\mp} + e_{z,1}^{\mp} \hat{\mathbf{z}}_1$ are the *normalized* electric and magnetic modal fields in the waveguide 1, derived from Eqs. (1) and (2) with the subscript 1. The walls of the waveguide are assumed to be perfectly conducting. From the reciprocity theorem (3), this technique was applied in [15–17] to obtain the coefficient A_1^+ for

rectangular and circular waveguides. In this paper, A_1^+ is derived for any canonical waveguide in appendix A and applied for a rectangular waveguide. Thus, the amplitudes $A_1^{+,\mathrm{h}}$ and $A_1^{+,\mathrm{e}}$ are related to the incident field via a matrix relation

$$\begin{bmatrix} A_1^{+,\mathrm{h}} \\ A_1^{+,\mathrm{e}} \end{bmatrix} = \frac{k_0}{2\sin\theta_i \beta_1^{\mathrm{h,e}} P_1^{\mathrm{h,e}}} \begin{bmatrix} Y_0\alpha_{\theta_i}^{\mathrm{h}} & Y_0\alpha_{\phi_i}^{\mathrm{h}} \\ \alpha_{\theta_i}^{\mathrm{e}} & \alpha_{\phi_i}^{\mathrm{e}} \end{bmatrix} \begin{bmatrix} E_{i\theta} \\ E_{i\phi} \end{bmatrix}. \tag{4}$$

The elements of the matrix are given by Eq. (A7) for any cross section Σ_1 and are *dimensionless*. They depend on the integrals $\{G_{x,y}^{\mathrm{h,e}}\}$ expressed from (A8), which can be derived analytically for a rectangular cross section. The substitution of Eq. (A14) into Eq. (A7) leads to

$$\begin{cases} \alpha_{\theta_i}^{\mathrm{h}} = -\left(k_{iy}^2 k_{n_1}^2 - k_{ix}^2 k_{m_1}^2\right)\left(1+\frac{\beta_1}{k_0}\cos\theta_i\right) G(k_{ix},a,n_1) G(k_{iy},b,m_1) \\ \alpha_{\phi_i}^{\mathrm{h}} = -k_{ix}k_{iy}\left(k_{n_1}^2 + k_{m_1}^2\right)\left(\frac{\beta_1}{k_0}+\cos\theta_i\right) G(k_{ix},a,n_1) G(k_{iy},b,m_1) \\ \alpha_{\theta_i}^{\mathrm{e}} = k_{n_1}k_{m_1}\left(k_{ix}^2 + k_{iy}^2\right)\left(\frac{\beta_1}{k_0}+\cos\theta_i\right) G(k_{ix},a,n_1) G(k_{iy},b,m_1) \\ \alpha_{\phi_i}^{\mathrm{e}} = 0 \end{cases}, \tag{5}$$

and

$$G(k,a,n_1) = -\frac{ja^2}{2\xi_\pm} e^{j\xi_\mp} \mathrm{sinc}\left(\xi_\mp\right) \quad \text{with} \quad \xi_\pm = \frac{a}{2}\left(k \pm k_{n_1}\right), \tag{6}$$

with (n_1, m_1) to be the mode indexes. In addition, $P_1^{\mathrm{h,e}}$ is given by Eq. (A11) and $\beta_1^{\mathrm{e}} = \beta_1^{\mathrm{h}} = \beta_1 = \sqrt{k_0^2 - k_{n_1}^2 - k_{m_1}^2}$, in which $k_{n_1} = \frac{n_1\pi}{a}$ and $k_{m_1} = \frac{m_1\pi}{b}$. The function $\mathrm{sinc}(x) = \sin(x)/x$ ($\mathrm{sinc}(0) = 1$) characterizes the diffraction by a rectangular aperture and it is commonly used to avoid the singularities. Indeed, if $\xi_+ > 0$, then the subscript — in Eq. (6) is used, and vice versa. This function allows also us to select easily the modes involved in the propagation.

2.3. Second Step — Reflection Matrix of the Waveguide 2

If the waveguide 1 is stuffed by a non-depolarizing and non-degenerative dielectric termination, the reflection matrix $\bar{\boldsymbol{\mathcal{R}}}_{is}$ is then

$$\begin{bmatrix} A_1^{-,\mathrm{h}} \\ A_1^{-,\mathrm{e}} \end{bmatrix} = \bar{\boldsymbol{\mathcal{R}}}_{is} \begin{bmatrix} A_1^{+,\mathrm{h}} \\ A_1^{+,\mathrm{e}} \end{bmatrix} e^{j\beta_1^{\mathrm{h,e}} L_1} = \begin{bmatrix} R^{\mathrm{hh}} & 0 \\ 0 & R^{\mathrm{ee}} \end{bmatrix} \begin{bmatrix} A_1^{+,\mathrm{h}} \\ A_1^{+,\mathrm{e}} \end{bmatrix} e^{j\beta_1^{\mathrm{h,e}} L_1}. \tag{7}$$

Since the termination is assumed to be non-depolarizing, the reflection matrix is diagonal. In addition, a non-degenerative termination implies that a mode (n_1, m_1) in the waveguide 1 is not converted into several modes in the waveguide 2. Thus, the coefficients $\{R^{\mathrm{hh}}, R^{\mathrm{ee}}\}$ are scalar. As shown in Fig. 1, if the waveguide 1 is connected to a bent waveguide 2, its effect can be studied by calculating the corresponding reflection matrix. By applying the same way as in the first step, this matrix can be derived by using a modal approach combined with the Kirchhoff approximation for the boundary conditions.

2.3.1. Derivation of the Transmitted Fields into the Waveguide 2

The starting point is to derive the transmitted mode amplitudes into the waveguide 2, $\{A_2^{+,\mathrm{h}}, A_2^{+,\mathrm{e}}\}$, via the reciprocity theorem given by

$$A_2^+ = -\frac{\displaystyle\int_{\Sigma_{12}} \left[\left(\mathbf{e}_{\mathrm{T},2}^- + \mathbf{e}_{z,2}^-\right)\cdot\mathbf{J}_{s1}^+ - \left(\mathbf{h}_{\mathrm{T},2}^- + \mathbf{h}_{z,2}^-\right)\cdot\mathbf{M}_{s1}^+\right] d\Sigma_{12}}{2\displaystyle\int_{\Sigma_{12}} \left(\mathbf{e}_{\mathrm{T},2}^- \wedge \mathbf{h}_{\mathrm{T},2}^-\right)\cdot\hat{\mathbf{n}}_{12} d\Sigma_{12}}, \quad (8)$$

with $\mathbf{e}_2^- = \mathbf{e}_{\mathrm{T},2}^- + e_{z,2}^-\hat{\mathbf{z}}_2$ and $\mathbf{h}_2^- = \mathbf{h}_{\mathrm{T},2}^- + e_{z,2}^-\hat{\mathbf{z}}_2$ the *reflected* electric and magnetic modal *normalized* fields onto the waveguide 2, derived from (1) and (2) with the subscript 2. On the surface Σ_{12}, $\mathbf{J}_{s1}^+ = \hat{\mathbf{n}}_{12}\wedge\mathbf{H}_1^+$ (electric) and $\mathbf{M}_{s1}^+ = -\hat{\mathbf{n}}_{12}\wedge\mathbf{E}_1^+$ (magnetic) are the currents, in which $\hat{\mathbf{n}}_{12}$ is the normal to the surface Σ_{12}. Using the Kirchhoff approximation on Σ_{12}, $\mathbf{E}_1^+ = \mathbf{E}_1^{+,\mathrm{h}} + \mathbf{E}_1^{+,\mathrm{e}}$ and $\mathbf{H}_1^+ = \mathbf{H}_1^{+,\mathrm{h}} + \mathbf{H}_1^{+,\mathrm{e}}$ are assumed to be the *transmitted modal* electric and magnetic fields in the waveguide 1, derived from Eqs. (1) and (2) multiplying by $\{A_1^{+,\mathrm{h}}, A_1^{+,\mathrm{e}}\}$ (according to the polarization) and with the subscript 1. The resulting equations are then

$$\begin{cases} E_{x,1}^+ = -\,j\left(A_1^{+,\mathrm{h}} e^{-j\beta^{\mathrm{h}}z} k_0 Z_0 \nabla_y \psi^{\mathrm{h}} + A_1^{+,\mathrm{e}} e^{-j\beta^{\mathrm{e}}z}\beta^{\mathrm{e}}\nabla_x\psi^{\mathrm{e}}\right)\Big|_1 \\ E_{y,1}^+ = +\,j\left(A_1^{+,\mathrm{h}} e^{-j\beta^{\mathrm{h}}z} k_0 Z_0 \nabla_x \psi^{\mathrm{h}} - A_1^{+,\mathrm{e}} e^{-j\beta^{\mathrm{e}}z}\beta^{\mathrm{e}}\nabla_y\psi^{\mathrm{e}}\right)\Big|_1 \\ E_{z,1}^+ = A_1^{+,\mathrm{e}} e^{-j\beta^{\mathrm{e}}z}(k_c^{\mathrm{e}})^2\psi^{\mathrm{e}}\Big|_1 \end{cases}, \quad (9)$$

and

$$\begin{cases} H_{x,1}^{+} = -j\left(A_1^{+,\mathrm{h}} e^{-j\beta^{\mathrm{h}} z}\beta^{\mathrm{h}}\nabla_x\psi^{\mathrm{h}} - A_1^{+,\mathrm{e}} e^{-j\beta^{\mathrm{e}} z} k_0 Y_0 \nabla_y \psi^{\mathrm{e}}\right)\Big|_1 \\ H_{y,1}^{+} = -j\left(A_1^{+,\mathrm{h}} e^{-j\beta^{\mathrm{h}} z}\beta^{\mathrm{h}}\nabla_y\psi^{\mathrm{h}} + A_1^{+,\mathrm{e}} e^{-j\beta^{\mathrm{e}} z} k_0 Y_0 \nabla_x \psi^{\mathrm{e}}\right)\Big|_1 \\ H_{z,1}^{+} = A_1^{+,\mathrm{h}} e^{-j\beta^{\mathrm{h}} z}(k_c^{\mathrm{h}})^2\psi^{\mathrm{h}}\Big|_1 \end{cases}, \quad (10)$$

with $\nabla_x = \frac{\partial}{\partial x}$, $\nabla_y = \frac{\partial}{\partial y}$, and the symbol $|_1$ means that the magnitudes are expressed in the waveguide 1.

From Fig. 1, we have

$$\begin{cases} \hat{\mathbf{n}}_{12} = \hat{\mathbf{z}}_2\cos\theta_2 - \hat{\mathbf{y}}_2\sin\theta_2 \\ \hat{\mathbf{z}}_1 = +\hat{\mathbf{z}}_2\cos\theta_{12} - \hat{\mathbf{y}}_2\sin\theta_{12} \\ \hat{\mathbf{y}}_1 = +\hat{\mathbf{z}}_2\sin\theta_{12} + \hat{\mathbf{y}}_2\cos\theta_{12} \\ \hat{\mathbf{x}}_1 = \hat{\mathbf{x}}_2 \end{cases}, \quad (11)$$

and the resulting vector dot products in the basis $(\hat{\mathbf{x}}_2, \hat{\mathbf{y}}_2, \hat{\mathbf{z}}_2)$ are then

$$\begin{cases} \mathbf{J}_{s1}^{+} = \left(-H_{y,1}^{+}\cos\theta_2 + H_{z,1}^{+}\sin\theta_2\right)\hat{\mathbf{x}}_2 \\ \qquad +H_{x,1}^{+}\cos\theta_2\hat{\mathbf{y}}_2 + H_{x,1}^{+}\sin\theta_2\hat{\mathbf{z}}_2 \\ -\mathbf{M}_{s1}^{+} = \left(-E_{y,1}^{+}\cos\theta_2 + E_{z,1}^{+}\sin\theta_2\right)\hat{\mathbf{x}}_2 \\ \qquad +E_{x,1}^{+}\cos\theta_2\hat{\mathbf{y}}_2 + E_{x,1}^{+}\sin\theta_2\hat{\mathbf{z}}_2 \end{cases}. \quad (12)$$

The scalar products in the numerator of Eq. (8) are then

$$\begin{cases} \left(\mathbf{e}_{\mathrm{T},2}^{-} + \mathbf{e}_{z,2}^{-}\right)\cdot\mathbf{J}_{s1}^{+} = \left(-H_{y,1}^{+}\cos\theta_2 + H_{z,1}^{+}\sin\theta_2\right)e_{x,2}^{-} \\ \qquad +H_{x,1}^{+}\cos\theta_2 e_{y,2}^{-} + H_{x,1}^{+}\sin\theta_2 e_{z,2}^{-} \\ -\left(\mathbf{h}_{\mathrm{T},2}^{-} + \mathbf{h}_{z,2}^{-}\right)\cdot\mathbf{M}_{s1}^{+} = \left(-E_{y,1}^{+}\cos\theta_2 + E_{z,1}^{+}\sin\theta_2\right)h_{x,2}^{-} \\ \qquad +E_{x,1}^{+}\cos\theta_2 h_{y,2}^{-} + E_{x,1}^{+}\sin\theta_2 h_{z,2}^{-}, \end{cases}. \quad (13)$$

From Eqs. (13), (10) and (9), the integrand of the numerator of Eq. (8) is for the TE case and according to $A_1^{+,\mathrm{h}}$

$$\begin{aligned} &\left(\mathbf{e}_{\mathrm{T},2}^{-} + \mathbf{e}_{z,2}^{-}\right)\cdot\mathbf{J}_{s1}^{+} - \left(\mathbf{h}_{\mathrm{T},2}^{-} + \mathbf{h}_{z,2}^{-}\right)\cdot\mathbf{M}_{s1}^{+} \\ &= k_0 Z_0 e^{j(\beta_2^{\mathrm{h}} z_2 - \beta_1^{\mathrm{h}} z_1)} A_1^{+,\mathrm{h}}\Big\{\cos\theta_2\left(\nabla_y\psi^{\mathrm{h}}\Big|_1\ \nabla_y\psi^{\mathrm{h}}\Big|_2\right. \\ &\quad \left.+\nabla_x\psi^{\mathrm{h}}\Big|_1\ \nabla_x\psi^{\mathrm{h}}\Big|_2\right)\left(\beta_1^{\mathrm{h}} + \beta_2^{\mathrm{h}}\right) \\ &\quad -j\sin\theta_2\left[\left(k_{c_1}^{\mathrm{h}}\right)^2\psi^{\mathrm{h}}\Big|_1\ \nabla_y\psi^{\mathrm{h}}\Big|_2 + \left(k_{c_2}^{\mathrm{e}}\right)^2\nabla_y\psi^{\mathrm{h}}\Big|_1\ \psi^{\mathrm{h}}\Big|_2\right]\Big\}, \end{aligned} \quad (14)$$

and according to $A_1^{+,\mathrm{e}}$

$$\begin{aligned}
&\left(\mathbf{e}_{\mathrm{T},2}^{-}+\mathbf{e}_{z,2}^{-}\right)\cdot\mathbf{J}_{s1}^{+}-\left(\mathbf{h}_{\mathrm{T},2}^{-}+\mathbf{h}_{z,2}^{-}\right)\cdot\mathbf{M}_{s1}^{+}\\
&=e^{j(\beta_2^{\mathrm{h}}z_2-\beta_1^{\mathrm{e}}z_1)}A_1^{+,\mathrm{e}}\Bigg\{\cos\theta_2\left(\nabla_x\psi^{\mathrm{e}}|_1\,\nabla_y\psi^{\mathrm{h}}\Big|_2\right.\\
&\left.-\nabla_y\psi^{\mathrm{e}}|_1\,\nabla_x\psi^{\mathrm{h}}\Big|_2\right)\left(k_0^2+\beta_1^{\mathrm{e}}\beta_2^{\mathrm{h}}\right)\\
&+j\sin\theta_2\left[\left(k_{c_1}^{\mathrm{e}}\right)^2\beta_2^{\mathrm{h}}\,\psi^{\mathrm{e}}|_1\,\nabla_x\psi^{\mathrm{h}}\Big|_2-\left(k_{c_2}^{\mathrm{h}}\right)^2\beta_1^{\mathrm{e}}\,\nabla_x\psi^{\mathrm{e}}|_1\,\psi^{\mathrm{h}}\Big|_2\right]\Bigg\}. \quad (15)
\end{aligned}$$

Using the same way for the TM polarization, it can be shown according to $A_1^{+,\mathrm{h}}$ that

$$\begin{aligned}
&\left(\mathbf{e}_{\mathrm{T},2}^{-}+\mathbf{e}_{z,2}^{-}\right)\cdot\mathbf{J}_{s1}^{+}-\left(\mathbf{h}_{\mathrm{T},2}^{-}+\mathbf{h}_{z,2}^{-}\right)\cdot\mathbf{M}_{s1}^{+}\\
&=\ e^{j(\beta_2^{\mathrm{e}}z_2-\beta_1^{\mathrm{h}}z_1)}A_1^{+,\mathrm{h}}\Bigg\{\cos\theta_2\left(\nabla_x\psi^{\mathrm{h}}\Big|_1\,\nabla_y\psi^{\mathrm{e}}|_2\right.\\
&\left.-\nabla_y\psi^{\mathrm{h}}\Big|_1\,\nabla_x\psi^{\mathrm{e}}|_2\right)\left(k_0^2+\beta_1^{\mathrm{h}}\beta_2^{\mathrm{e}}\right)\\
&+j\sin\theta_2\left[\left(k_{c_1}^{\mathrm{h}}\right)^2\beta_2^{\mathrm{e}}\,\psi^{\mathrm{h}}\Big|_1\nabla_x\psi^{\mathrm{e}}|_2-\left(k_{c_2}^{\mathrm{e}}\right)^2\beta_1^{\mathrm{h}}\,\nabla_x\psi^{\mathrm{h}}\Big|_1\,\psi^{\mathrm{e}}|_2\right]\Bigg\}, \quad (16)
\end{aligned}$$

and according to $A_1^{+,\mathrm{e}}$

$$\begin{aligned}
&\left(\mathbf{e}_{\mathrm{T},2}^{-}+\mathbf{e}_{z,2}^{-}\right)\cdot\mathbf{J}_{s1}^{+}-\left(\mathbf{h}_{\mathrm{T},2}^{-}+\mathbf{h}_{z,2}^{-}\right)\cdot\mathbf{M}_{s1}^{+}\\
&=\ k_0Y_0e^{j(\beta_2^{\mathrm{e}}z_2-\beta_1^{\mathrm{e}}z_1)}A_1^{+,\mathrm{e}}\Bigg\{-\cos\theta_2\left(\nabla_y\psi^{\mathrm{e}}|_1\,\nabla_y\psi^{\mathrm{e}}|_2\right.\\
&\left.+\nabla_x\psi^{\mathrm{e}}|_1\,\nabla_x\psi^{\mathrm{e}}|_2\right)\left(\beta_1^{\mathrm{e}}+\beta_2^{\mathrm{e}}\right)\\
&+j\sin\theta_2\left[\left(k_{c_1}^{\mathrm{e}}\right)^2\psi^{\mathrm{e}}|_1\,\nabla_y\psi^{\mathrm{e}}|_2+\left(k_{c_2}^{\mathrm{e}}\right)^2\nabla_y\psi^{\mathrm{e}}|_1\,\psi^{\mathrm{e}}|_2\right]\Bigg\}. \quad (17)
\end{aligned}$$

Moreover, the denominator of Eq. (8) can be written as

$$\begin{aligned}
\int_{\Sigma_{12}}\left(\mathbf{e}_{\mathrm{T},2}^{-}\wedge\mathbf{h}_{\mathrm{T},2}^{-}\right)\cdot\hat{\mathbf{n}}_{12}d\Sigma_{12}\ =\ &\cos\theta_2\beta^{\mathrm{h,e}}k_0\times\int_{\Sigma_{12}}e^{2j\beta^{\mathrm{h,e}}z}\left[\left(\nabla_x\psi^{\mathrm{h,e}}\right)^2\right.\\
&\left.+\left(\nabla_y\psi^{\mathrm{h,e}}\right)^2\right]d\Sigma_{12}\Bigg|_2\begin{cases}Z_0 & \mathrm{TE}\\ Y_0 & \mathrm{TM}\end{cases}, \quad (18)
\end{aligned}$$

with $\hat{\mathbf{z}}_2\cdot\hat{\mathbf{n}}_{12}=\cos\theta_2$ and

$$\int_{\Sigma_{12}}d\Sigma_{12}=\int_{\Sigma_{12}}dx_{12}dy_{12}=\frac{1}{\cos\theta_2}\int_0^a dx_2\int_0^{b\cos\theta_2}dy_2. \quad (19)$$

A depolarizing effect occurs at the bend discontinuity, which implies that for TE and TM polarizations, TM and TE modes appear, respectively, in the waveguide 2. If the bend disappears, then $\theta_2 = 0$, $\beta_1^{\mathrm{h,e}} = \beta_2^{\mathrm{h,e}}$, and since $\nabla_x\psi^{\mathrm{e}}\nabla_y\psi^{\mathrm{h}} - \nabla_y\psi^{\mathrm{e}}\nabla_x\psi^{\mathrm{h}} = 0$ (orthogonally relation between the eigen functions), one can show that $A_2^{+,\mathrm{h}} = A_1^{+,\mathrm{h}}e^{j\beta^{\mathrm{h}}L_1}$ and $A_2^{+,\mathrm{e}} = A_1^{+,\mathrm{e}}e^{j\beta^{\mathrm{e}}L_1}$, where L_1 is the length of the waveguide 1.

2.3.2. Case of Rectangular Waveguides

If the waveguides 1 and 2 have a same rectangular cross section, then Eqs. (14)–(17) can be simplified. Indeed, in this case, $\psi_1^{\mathrm{h,e}} = \psi_2^{\mathrm{h,e}}$ (but their arguments are different), $\beta^{\mathrm{h}} = \beta^{\mathrm{e}} = \beta$ and $k_c^{\mathrm{h}} = k_c^{\mathrm{e}} = k_c$. On the other hand, since β and k_c depend on the mode indexes (n, m), they are different in each waveguide.

From Eqs. (8) and (9), the derivation of the transmitted coefficients $\{A_2^{+,\mathrm{h}}, A_2^{+,\mathrm{e}}\}$ require the calculation of two integrations over x_2 and y_2. This is done in Appendix C, and the resulting equation is then

$$\begin{bmatrix} A_2^{+,\mathrm{h}} \\ A_2^{+,\mathrm{e}} \end{bmatrix} = e^{j\beta_1 L_1} \begin{bmatrix} T_{12}^{\mathrm{hh}} & Y_0 T_{12}^{\mathrm{he}} \\ Z_0 T_{12}^{\mathrm{eh}} & T_{12}^{\mathrm{ee}} \end{bmatrix} \begin{bmatrix} A_1^{+,\mathrm{h}} \\ A_1^{+,\mathrm{e}} \end{bmatrix}, \tag{20}$$

with

$$\begin{aligned} P_{12}^{\mathrm{h}} T_{12}^{\mathrm{hh}} = &+ \cos\theta_2 \left(\beta_1 + \beta_2\right) \left(k_{n_1} k_{n_2} G_{12}^{++} - k_{m_1} k_{m_2} G_{12}^{--}\right) \\ &+ \sin\theta_2 \left(k_{c_1}^2 k_{m_2} G_{12}^{+-} + k_{c_2}^2 k_{m_1} G_{12}^{-+}\right), \end{aligned} \tag{21}$$

$$\begin{aligned} k_0 P_{12}^{\mathrm{h}} T_{12}^{\mathrm{he}} = &+ \cos\theta_2 \left(k_0^2 + \beta_1\beta_2\right) \left(k_{m_1} k_{n_2} G_{12}^{++} + k_{m_2} k_{n_1} G_{12}^{--}\right) \\ &- \sin\theta_2 \left(k_{c_1}^2 k_{n_2}\beta_2 + k_{c_2}^2 k_{n_1}\beta_1\right) G_{12}^{-+}, \end{aligned} \tag{22}$$

$$\begin{aligned} k_0 P_{12}^{\mathrm{e}} T_{12}^{\mathrm{eh}} = &- \cos\theta_2 \left(k_0^2 + \beta_1\beta_2\right) \left(k_{m_1} k_{n_2} G_{12}^{--} + k_{m_2} k_{n_1} G_{12}^{++}\right) \\ &+ \sin\theta_2 \left(k_{c_1}^2 k_{n_2}\beta_2 + k_{c_2}^2 k_{n_1}\beta_1\right) G_{12}^{+-}, \end{aligned} \tag{23}$$

and

$$\begin{aligned} P_{12}^{\mathrm{e}} T_{12}^{\mathrm{ee}} = &+ \cos\theta_2 \left(\beta_1 + \beta_2\right) \left(k_{n_1} k_{n_2} G_{12}^{--} - k_{m_1} k_{m_2} G_{12}^{++}\right) \\ &+ \sin\theta_2 \left(k_{c_1}^2 k_{m_2} G_{12}^{-+} + k_{c_2}^2 k_{m_1} G_{12}^{+-}\right). \end{aligned} \tag{24}$$

Moreover

$$\begin{cases} P_{12}^{\mathrm{h}} = -2\beta_2 \cos\theta_2 \left(k_{n_2}^2 G'^{++}_{12} - k_{m_2}^2 G'^{--}_{12} \right) \\ P_{12}^{\mathrm{e}} = -2\beta_2 \cos\theta_2 \left(k_{m_2}^2 G'^{++}_{12} - k_{n_2}^2 G'^{--}_{12} \right) \end{cases} . \tag{25}$$

It should be noted that $k_{n_1} = k_{n_2} = k_n = \frac{n\pi}{a}$ $(n = n_1 = n_2)$, $k_{m_i} = \frac{m_i \pi}{b}$, $\beta_i = \sqrt{k_0^2 - k_{n_i}^2 - k_{m_i}^2}$ and $k_{c_i}^2 = k_{n_i}^2 + k_{m_i}^2$. In addition, $G_{12}^{p_1 p_2}$ is defined by (C12), $G'^{p_1 p_2}_{12} = G_{12}^{p_1 p_2}|_{m_1 = m_2}$ $(\beta_1 = \beta_2, k_{m_1} = k_{m_2})$, and $\{T_{ij}\}$ are *dimensionless*.

If the tilt angle of the bend equals zero, $\theta_{12} = 0$, then the argument of the $G_{12}^{p_1 p_2}$ function is $\xi_{12}^{s_1 s_2} = \frac{\pi}{2}(s_1 m_1 + s_2 m_2)$, in which $s_1 m_1 + s_2 m_2$ is an integer. From (C12), it can then be shown that

$$\begin{cases} G_{12}^{++} = \frac{1}{2}\left(\delta_{m_1+m_2,0} + \delta_{m_1,m_2}\right) \\ G_{12}^{--} = \frac{1}{2}\left(\delta_{m_1+m_2,0} - \delta_{m_1,m_2}\right) \\ G_{12}^{+-} = \begin{cases} 0 & \text{if} \quad m_1 + m_2 \quad \text{odd} \\ +\frac{2m_2}{\pi(m_2^2 - m_1^2)} & \text{otherwise} \end{cases} \\ G_{12}^{-+} = \begin{cases} 0 & \text{if} \quad m_1 + m_2 \quad \text{odd} \\ -\frac{2m_1}{\pi(m_2^2 - m_1^2)} & \text{otherwise} \end{cases} \end{cases} . \tag{26}$$

2.3.3. Derivation of the Reflected Fields onto the Waveguide 2

If the waveguide 2 is stuffed by a non-depolarizing and non-degenerative dielectric termination, the reflection coefficients in the waveguide 2 are then

$$\begin{bmatrix} A_2^{-,\mathrm{h}} \\ A_2^{-,\mathrm{e}} \end{bmatrix} = \begin{bmatrix} R^{\mathrm{hh}} & 0 \\ 0 & R^{\mathrm{ee}} \end{bmatrix} \begin{bmatrix} A_2^{+,\mathrm{h}} \\ A_2^{+,\mathrm{e}} \end{bmatrix} e^{j\beta_2^{\mathrm{h,e}} L_2}. \tag{27}$$

2.3.4. Derivation of the Reflected Fields onto the Waveguide 1

Again, the reciprocity theorem is applied for the derivation of A_1^-. Using the same way as the calculation of A_2^+, it can be shown that

$$\begin{bmatrix} A_1^{-,\mathrm{h}} \\ A_1^{-,\mathrm{e}} \end{bmatrix} = e^{j\beta_2 L_2} \begin{bmatrix} T_{21}^{\mathrm{hh}} & Y_0 T_{21}^{\mathrm{he}} \\ Z_0 T_{21}^{\mathrm{eh}} & T_{21}^{\mathrm{ee}} \end{bmatrix} \begin{bmatrix} A_2^{-,\mathrm{h}} \\ A_2^{-,\mathrm{e}} \end{bmatrix}, \tag{28}$$

with

$$\begin{cases} P_{21}^{\mathrm{h}} T_{21}^{\mathrm{hh}} = P_{12}^{\mathrm{h}} T_{12}^{\mathrm{hh}} & P_{21}^{\mathrm{h}} T_{21}^{\mathrm{he}} = P_{12}^{\mathrm{h}} T_{12}^{\mathrm{he}} \\ P_{21}^{\mathrm{e}} T_{21}^{\mathrm{eh}} = P_{12}^{\mathrm{e}} T_{12}^{\mathrm{eh}} & P_{21}^{\mathrm{h}} T_{21}^{\mathrm{hh}} = P_{12}^{\mathrm{h}} T_{12}^{\mathrm{hh}} \end{cases} , \tag{29}$$

and

$$\begin{cases} P_{21}^{\mathrm{h}} = -2\beta_1 \cos\theta_1 \left(k_{n_1}^2 G'^{++}_{21} - k_{m_1}^2 G'^{--}_{21} \right) \\ P_{21}^{\mathrm{e}} = -2\beta_1 \cos\theta_1 \left(k_{m_1}^2 G'^{++}_{21} - k_{n_1}^2 G'^{--}_{21} \right) \end{cases} . \tag{30}$$

It should be noted that $G_{21}^{p_1p_2} = G_{12}^{p_1p_2}$ defined by (C12) and $G'^{p_1p_2}_{21} = G'^{p_1p_2}_{12} = G_{12}^{p_1p_2}|_{m_1=m_2}$ ($\beta_1 = \beta_2$, $k_{m_1} = k_{m_2}$).

2.3.5. Conclusion — Reflection Matrix of the Waveguide 2

In conclusion, from Eqs. (20), (27) and (28) the reflection matrix defined by Eq. (7) is expressed as

$$\bar{\boldsymbol{\mathcal{R}}}_{is} = \begin{bmatrix} R^{\mathrm{hh}}T_{12}^{\mathrm{hh}}T_{21}^{\mathrm{hh}} + R^{\mathrm{ee}}T_{12}^{\mathrm{eh}}T_{21}^{\mathrm{he}} & R^{\mathrm{hh}}T_{12}^{\mathrm{he}}T_{21}^{\mathrm{hh}} + R^{\mathrm{ee}}T_{12}^{\mathrm{ee}}T_{21}^{\mathrm{he}} \\ R^{\mathrm{hh}}T_{12}^{\mathrm{hh}}T_{21}^{\mathrm{eh}} + R^{\mathrm{ee}}T_{12}^{\mathrm{eh}}T_{21}^{\mathrm{ee}} & R^{\mathrm{hh}}T_{12}^{\mathrm{he}}T_{21}^{\mathrm{eh}} + R^{\mathrm{ee}}T_{12}^{\mathrm{ee}}T_{21}^{\mathrm{ee}} \end{bmatrix}, \tag{31}$$

and in Eq. (7), the phase term $e^{j\beta_1 L_1}$ ($\beta_1 = \beta_1^{\mathrm{h}} = \beta_1^{\mathrm{e}}$) is substituted for $e^{j\beta_1 L_1 + 2j\beta_2 L_2}$. If the tilt angle of the bend equals zero, $\theta_{12} = 0$, then from Eqs. (21)–(24), (26), (29), and (30), it can be shown that $T_{12}^{\mathrm{he}} = T_{12}^{\mathrm{eh}} = T_{21}^{\mathrm{he}} = T_{21}^{\mathrm{eh}} = 0$, $T_{12}^{\mathrm{hh}}T_{21}^{\mathrm{hh}} = T_{12}^{\mathrm{ee}}T_{21}^{\mathrm{ee}} = \delta_{m_1,m_2}$. This implies that the matrix $\bar{\boldsymbol{\mathcal{R}}}_{is}$ is diagonal, whose elements are $R^{\mathrm{hh}}\delta_{m_1,m_2}$ and $R^{\mathrm{ee}}\delta_{m_1,m_2}$.

2.4. Third Step — Electromagnetic Fields Radiated by the Waveguide 1

From Appendix B, the components of the scattered field in far zone, $(E_{s\theta}, E_{s\phi})$, are expressed from the amplitudes of the *reflected* modes onto the waveguide 1, $\{A_1^{-,\mathrm{h}}, A_1^{-,\mathrm{e}}\}$ by a matrix relation

$$\begin{bmatrix} E_{s\theta} \\ E_{s\phi} \end{bmatrix} = \frac{je^{-jk_0R_0}}{4\pi k_0 R_0} \begin{bmatrix} Z_0\alpha_{\theta_s}^{\mathrm{h}} & Z_0\alpha_{\theta_s}^{\mathrm{e}} \\ \alpha_{\phi_s}^{\mathrm{h}} & \alpha_{\phi_s}^{\mathrm{e}} \end{bmatrix} \begin{bmatrix} A_1^{-,\mathrm{h}} \\ A_1^{-,\mathrm{e}} \end{bmatrix} e^{j\beta_1^{\mathrm{h,e}}L_1}. \tag{32}$$

The elements of the matrix are given by Eq. (B5) for any cross section Σ_1. They depend on the integrals $\{G_{x,y}^{\mathrm{h,e}}\}$ expressed from (A8), which can be derived analytically for a rectangular cross section (see Eq. (A14)). Comparing then, Eq. (B5) with (A7), it is interesting to

note that

$$\begin{cases} \alpha_{\theta_s}^{\mathrm{h}} = -\left.\alpha_{\theta_i}^{\mathrm{h}}\right|_{\theta_i=\theta_s,\phi_i=\phi_s} \\ \alpha_{\phi_s}^{\mathrm{h}} = -\left.\alpha_{\phi_i}^{\mathrm{h}}\right|_{\theta_i=\theta_s,\phi_i=\phi_s} \\ \alpha_{\theta_s}^{\mathrm{e}} = \left.\alpha_{\theta_i}^{\mathrm{e}}\right|_{\theta_i=\theta_s,\phi_i=\phi_s} \\ \alpha_{\phi_s}^{\mathrm{e}} = \left.\alpha_{\phi_i}^{\mathrm{e}}\right|_{\theta_i=\theta_s,\phi_i=\phi_s} \end{cases} . \tag{33}$$

2.5. Last Step — Sinclair Matrix of the Cavity

In conclusion, for the open ended cavity presented in Fig. 1, the Sinclair matrix, $\bar{\boldsymbol{\mathcal{S}}}$, which links the component of the scattered fields $\{E_{s\theta}, E_{s\phi}\}$ to that of the incident fields $\{E_{i\theta}, E_{i\phi}\}$, is expressed from Eqs. (7) (matrix $\bar{\boldsymbol{\mathcal{R}}}_{is}$ is given by (31)), (4) and (32) as

$$\begin{bmatrix} E_{s\theta} \\ E_{s\phi} \end{bmatrix} = \begin{bmatrix} E_{i\theta} \\ E_{i\phi} \end{bmatrix} \frac{je^{-jk_0R_0}}{4\pi k_0 R_0} \bar{\boldsymbol{\mathcal{S}}}, \tag{34}$$

with

$$\bar{\boldsymbol{\mathcal{S}}} = \left.\bar{\boldsymbol{\mathcal{T}}}_{01}^{\mathrm{T}}\right|_{\theta_s,\phi_s} \underbrace{\bar{\boldsymbol{\mathcal{T}}}_{21}\bar{\boldsymbol{\mathcal{R}}}\bar{\boldsymbol{\mathcal{T}}}_{12}}_{\bar{\boldsymbol{\mathcal{R}}}_{is}} \left.\bar{\boldsymbol{\mathcal{T}}}_{01}\right|_{\theta_i,\phi_i} . \tag{35}$$

The transmission matrices are expressed as

$$\bar{\boldsymbol{\mathcal{T}}}_{ij} = \begin{bmatrix} T_{ij}^{\mathrm{hh}} & T_{ij}^{\mathrm{he}} \\ T_{ij}^{\mathrm{eh}} & T_{ij}^{\mathrm{ee}} \end{bmatrix} e^{j\beta_2 L_2}, \tag{36}$$

$$\left.\bar{\boldsymbol{\mathcal{T}}}_{01}\right|_{\theta_i,\phi_i} = \frac{1}{\sin\theta_i}\sqrt{\frac{k_0}{2P_1\beta_1}} \left.\begin{bmatrix} \alpha_\theta^{\mathrm{h}} & \alpha_\phi^{\mathrm{h}} \\ \alpha_\theta^{\mathrm{e}} & \alpha_\phi^{\mathrm{e}} \end{bmatrix}\right|_{\theta=\theta_i,\phi=\phi_i} e^{j\beta L_1}, \tag{37}$$

$$\left.\bar{\boldsymbol{\mathcal{T}}}_{01}^{\mathrm{T}}\right|_{\theta_s,\phi_s} = \frac{1}{\sin\theta_s}\sqrt{\frac{k_0}{2P_1\beta_1}} \left.\begin{bmatrix} -\alpha_\theta^{\mathrm{h}} & \alpha_\theta^{\mathrm{e}} \\ -\alpha_\phi^{\mathrm{h}} & \alpha_\phi^{\mathrm{e}} \end{bmatrix}\right|_{\theta=\theta_s,\phi=\phi_s} e^{j\beta L_1}, \tag{38}$$

whose the elements are given by Eqs. (21)–(24), (29) and (5). In addition, the matrix $\bar{\boldsymbol{\mathcal{R}}}$ is defined as

$$\bar{\boldsymbol{\mathcal{R}}} = \begin{bmatrix} R^{\mathrm{hh}} & 0 \\ 0 & R^{\mathrm{ee}} \end{bmatrix}. \tag{39}$$

For a monostatic configuration, $\theta = \theta_i = \theta_s$ and $\phi = \phi_i = \phi_s$, and for a rectangular cross section Σ_1, $\alpha_\phi^{\rm e} = 0$, the elements of the Sinclair matrix are

$$\bar{\boldsymbol{\mathcal{S}}} = \begin{bmatrix} -R_{is}^{\rm hh}\left(\alpha_\theta^{\rm h}\right)^2 + R_{is}^{\rm ee}\left(\alpha_\theta^{\rm e}\right)^2 + \alpha_\theta^{\rm h}\alpha_\theta^{\rm e}\left(R_{is}^{\rm eh} - R_{is}^{\rm he}\right) & \alpha_\phi^{\rm h}\left(R_{is}^{\rm eh}\alpha_\theta^{\rm e} - R_{is}^{\rm hh}\alpha_\theta^{\rm h}\right) \\ -\alpha_\phi^{\rm h}\left(R_{is}^{\rm he}\alpha_\theta^{\rm e} + R_{is}^{\rm hh}\alpha_\theta^{\rm h}\right) & -R_{is}^{\rm hh}\left(\alpha_\phi^{\rm h}\right)^2 \end{bmatrix}, \tag{40}$$

where the elements $\{R_{is}^{\rm hh}, R_{is}^{\rm he}, R_{is}^{\rm eh}, R_{is}^{\rm ee}\}$ are given by (31) and are *dimensionless*.

Equation (34) corresponds to the scattered field by a *single* mode (n, m_1, m_2) with $n = n_1 = n_2$. Thus, in far-field, the Radar Cross Section (RCS) in $\rm m^2$ is then

$$\sigma_{ij} = \frac{1}{4\pi k_0^2}\left|\sum_n \sum_{m_1} \sum_{m_2} S_{ij}\right|^2. \tag{41}$$

with $i = \{\theta, \phi\}$ and $j = \{\theta, \phi\}$, and $\{S_{ij}\}$ the elements of the $\bar{\boldsymbol{\mathcal{S}}}$ matrix.

3. GENERALIZATION TO $N_{\rm wg}$ CONNECTED WAVEGUIDES

This section is devoted to the generalization of the formulation to $N_{\rm wg}$ connected rectangular waveguides of same cross section and uniforms along the $\hat{\mathbf{z}}$ direction, and stuffed by a non-degenerative and non-depolarizing termination. An example of a such structure is depicted in Fig. 2. Each waveguide has a length L_p ($p \in [1; N_{\rm wg}]$), and each bend is characterized by this tilt angle $\theta_{p-1,p}$ ($p \in [2; N_{\rm wg}]$), which is defined along the constant $\hat{\mathbf{z}}$ direction and in the plane $(\hat{\mathbf{z}}, \hat{\mathbf{y}})$).

For $N_{\rm wg}$ connected rectangular waveguides, Eq. (35) becomes with $p' = p + 1$

$$\bar{\boldsymbol{\mathcal{S}}} = \bar{\boldsymbol{\mathcal{T}}}_{01}^{\rm T}\Big|_{\theta_s,\phi_s} \underbrace{\left(\prod_{p=1}^{p=N_{\rm wg}-1} \bar{\boldsymbol{\mathcal{T}}}_{p'p}\bar{\boldsymbol{\mathcal{R}}}\bar{\boldsymbol{\mathcal{T}}}_{pp'}\right)}_{\bar{\boldsymbol{\mathcal{R}}}_{is}} \bar{\boldsymbol{\mathcal{T}}}_{01}\Big|_{\theta_i,\phi_i}. \tag{42}$$

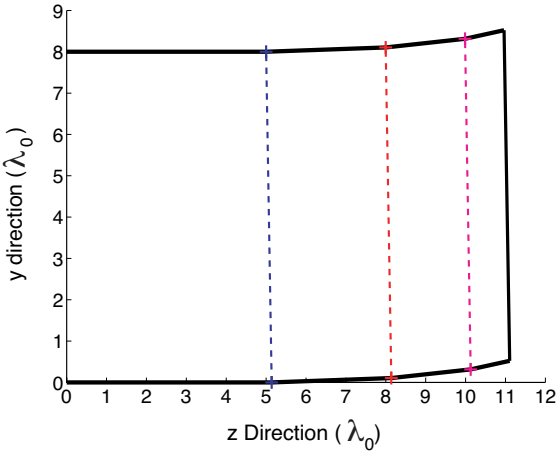

Figure 2. Cavity of rectangular and *uniform* cross section along the $\hat{\mathbf{z}}$ direction, and modeled as a succession of 3 bends. $b_1 = 8\lambda_0$ ($a_1 = 8\lambda_0$), $L_1 = 5\lambda_0$, $L_2 = 3\lambda_0$, $L_3 = 2\lambda_0$, $L_4 = 1\lambda_0$, $\theta_{12} = 2^{\rm o}$, $\theta_{23} = 4^{\rm o}$ et $\theta_{34} = 6^{\rm o}$ ($\theta_{r,12} = \theta_{r,23} = \theta_{r,34} = 2^{\rm o}$).

It should be noted that the elements of the matrix $\bar{\boldsymbol{\mathcal{T}}}_{pp'}$ depend on the mode indexes $(n, m_p, m_{p'})$ ($n_1 = n_2 = n$), whereas the elements of the matrix $\bar{\boldsymbol{\mathcal{T}}}_{01}$ depend on (n, m_1).

The RCS is then

$$\begin{aligned}\sigma_{ij} &= \frac{4\pi}{k_0^2}\left|\sum_n\sum_{m_1}\sum_{m_2}\cdots\sum_{m_{N_{\rm wg}}} S_{ij}\right|^2 \\ &= \frac{4\pi}{k_0^2}\left|\sum_n\sum_{m_1}\bar{\boldsymbol{\mathcal{T}}}_{01}^{\rm T}\Big|_{\theta_s,\phi_s}\left(\sum_{m_2}\bar{\boldsymbol{\mathcal{T}}}_{21}\Big[\sum_{m_3}\bar{\boldsymbol{\mathcal{T}}}_{32}\Big\{\cdots\sum_{m_{N_{\rm wg}}}\right.\right. \\ &\quad \left.\left.\bar{\boldsymbol{\mathcal{T}}}_{N_{\rm wg},N_{\rm wg}-1}\bar{\boldsymbol{\mathcal{R}}}\bar{\boldsymbol{\mathcal{T}}}_{N_{\rm wg}-1,N_{\rm wg}}\cdots\Big\}\bar{\boldsymbol{\mathcal{T}}}_{23}\Big]\bar{\boldsymbol{\mathcal{T}}}_{12}\right)\bar{\boldsymbol{\mathcal{T}}}_{01}\Big|_{\theta_i,\phi_i}\right|^2. \quad (43)\end{aligned}$$

If the tilt angles $\{\theta_{p-1,p}\} = \{0\}$, then $\bar{\boldsymbol{\mathcal{T}}}_{ij} = \bar{\boldsymbol{\mathcal{T}}}_{ji}$, which is a *diagonal* matrix whose the elements equal δ_{m_i,m_j}. Thus, the sum computations over $\{m_i\}$ with $i \in [2; N_{\rm wg}]$ are not necessary and the matrix product is reduced to $\bar{\boldsymbol{\mathcal{T}}}_{01}^{\rm T}\Big|_{\theta_s,\phi_s}\bar{\boldsymbol{\mathcal{R}}}\,\bar{\boldsymbol{\mathcal{T}}}_{01}\Big|_{\theta_i,\phi_i}$.

4. NUMERICAL RESULTS

In this section, numerical results of the monostatic RCS are shown in co-polarizations, $\sigma_{\theta\theta}$ and $\sigma_{\phi\phi}$. In addition, they are compared with the Iterated Physical Optics (IPO) method [14] and the Multi-Level Fast Multipole Method (MLFMM) generated by the commercial software FEKO [21]. The MLFMM is based on the MoM and has the advantage to solve electromagnetic problem with many unknowns comparatively to the MoM. To be consistent with the Kirchhoff approximation, the dimensions of the aperture Σ_0, (a_1, b_1), must be large comparatively to the wavelength λ_0. Typically, $a_1 \geq 5\lambda_0$ and $b_1 \geq 5\lambda_0$ [18]. On the other hand, on a standard PC, the MLFMM is limited to cavity of dimensions $8\lambda_0 \times 8\lambda_0 \times 9\lambda_0$ with a sampling step of $\lambda_0/8$. The frequency is $f = 10\,\mathrm{GHz}$, i.e., $\lambda_0 = 3\,\mathrm{cm}$.

4.1. Selective Modal Scheme for the Waveguide 1

For a large aperture, the number of modes (n_1, m_1) contributing to the RCS can be great, and thus the computing time of the sums over (n_1, m_1) can be very long. To decrease this time, a selective modal scheme similar to the one addressed in [16] is applied in the waveguide 1.

For the waveguide 1, the elements of the matrix $\bar{\boldsymbol{\mathcal{T}}}_{01}$ given by Eq. (5) depending on the G function expressed from Eq. (6). This function depends on $\mathrm{sinc}\,(\xi_{\mp})$, which is a decreasing function of $\xi_{\mp} = \frac{a}{2}(k_{x,y} \mp k_{n_1,m_1})$. The wavenumber k either equals $k_x = k_0 \sin\theta\cos\phi \geq 0$ (with k_{n_1}) or equals $k_y = k_0 \sin\theta\sin\phi \geq 0$ (with k_{m_1}), with $\theta = \theta_i = \theta_s \geq 0$ and $\phi = \phi_i = \phi_s \geq 0$. In Eq. (6), taking the subscript $-$ in $\xi_{\mp}$ to avoid the division by zero owing to $\frac{1}{\xi_{\pm}}$ $(\xi_+ > 0)$, the function $|G|$ decreases rapidly as ξ_- increases and is maximum for $\xi_- = 0$ $(\mathrm{sinc}(0) = 1)$. Thus, chosen an integer defined as $\frac{\xi_-}{\pi} = p_1 > 0$, the set of the modes $(n_1 \in [n_{1,\min}; n_{1,\max}], m_1 \in [m_{1,\min}; m_{1,\max}])$ contributing to the scattering can be defined as

$$\begin{cases} n_{1,\min} = \lfloor n_{10} \rfloor_- - 2p_1 & n_{1,\max} = \lfloor n_{10} \rfloor_- + 2p_1 \\ m_{1,\min} = \lfloor m_{10} \rfloor_- - 2p_1 & m_{1,\max} = \lfloor m_{10} \rfloor_- + 2p_1 \end{cases}, \tag{44}$$

with

$$n_{10} = \frac{2a}{\lambda_0}\sin\theta\cos\phi \quad m_{10} = \frac{2b}{\lambda_0}\sin\theta\sin\phi, \tag{45}$$

and $n_1 \geq 0$ and $m_1 \geq 0$. The function $\lfloor x \rfloor_-$ rounds the variable x to the nearest integer towards zero. The numbers n_{10} and m_{10} are

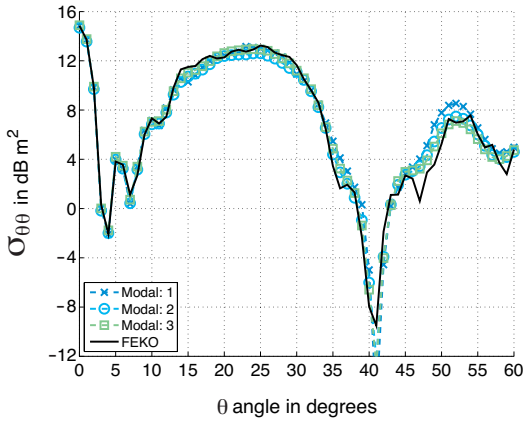

Figure 3. Monostatic RCS $\sigma_{\theta\theta}$ in dB m^2 versus θ and $p_1 = \{1, 2, 3\}$. $a_1 = b_1 = 8\lambda_0$, $L_1 = 9\lambda_0$, and $\phi = 0$.

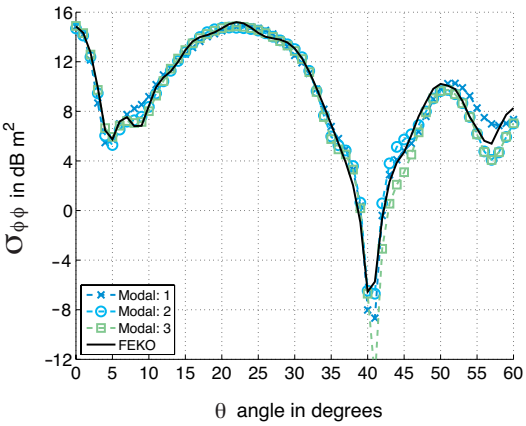

Figure 4. Same as in Fig. 3 but for $\sigma_{\phi\phi}$.

defined such as $\frac{\xi_-}{\pi} = 0$ with $\xi_- = \frac{a}{2}(k_x - k_{n_1})$ and $\xi_- = \frac{b}{2}(k_y - k_{m_1})$, respectively.

Figures 3 and 4 present the monostatic RCS $\sigma_{\theta\theta}$ and $\sigma_{\phi\phi}$ in dB m^2, respectively, versus θ and $p_1 = \{1, 2, 3\}$. In addition, the results obtained from FEKO are shown. $a_1 = b_1 = 8\lambda_0$, $L_1 = 9\lambda_0$, and $\phi = 0$. In the legend, "Modal: p_1" denotes our method and p_1 is the value used in Eq. (44) to select the mode indexes which contribute to the scattering. The corresponding values of $n_{1,\min}$ and $n_{1,\max}$ are presented in Fig. 5 versus θ.

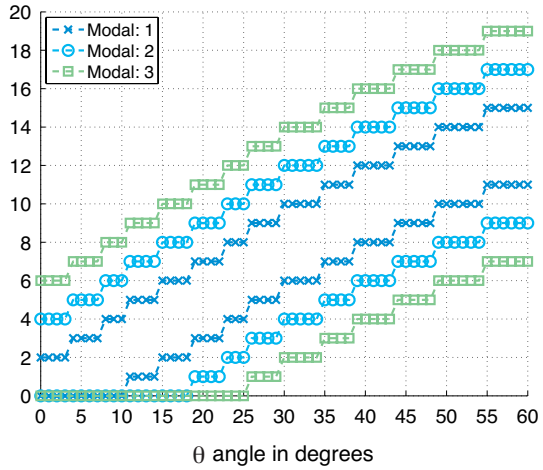

Figure 5. Values $\max(n_1)$ and $\min(n_1)$, computed from Eq. (44), versus θ and used for the RCS presented in Figs. 3 and 4.

For $p_1 = 3$, a very good agreement is obtained with the FEKO results. For $p_1 = 4$, the RCSs (not reported in this paper) are the same as that computed for $p_1 = 3$. From Fig. 5, as the angle θ increases, the mode indexes contributing to the scattering increase because $\sin\theta$ is an increasing of $\theta \in [0; \pi/2]$. In addition, for $p_1 = \{1, 2, 3\}$ and from θ values larger than $\theta = \{10, 18, 25\}^\circ$, $\Delta n_1 = n_{1,\max} - n_{1,\min} = 4p_1 = \{4, 8, 12\}$ is a constant with respect to θ. It should be noted that since $\phi = 0$, $m_{10} = 0$, $m_{1,\min} = 0$ and $p_{1,\max} = \Delta m_1 = 2p_1$ for any θ. For the next simulations, $p_1 = 3$.

As a conclusion, this efficient procedure allows us to reduce the term number in the computation of the sums over n_1 and m_1.

The evanescent modes occur for $\beta_1^2 < 0$, which implies for $a_1 = b_1$ that $\frac{4a_1^2}{\lambda_0^2} < n_1^2 + m_1^2$. Thus in Figs. 3 and 4, the modes for which $n_1^2 + m_1^2 > 256$ are evanescent. For instance, for $\theta = 25^\circ$ and $p_1 = 3$, from Fig. 5, $n_{1,\max} = 12$, $m_{1,\max} = 6$, and then, all the modes are propagative since $n_{1,\max}^2 + m_{1,\max}^2 = 180 < 256$. As a contrast, for $\theta = 50^\circ$, $n_{1,\max} = 18$, $n_{1,\max}^2 + m_{1,\max}^2 = 360 > 256$, and then, a part of the modes are evanescent.

4.2. Selective Modal Scheme for the Waveguide 2

In this subsection, the selective modal scheme is generalized to the waveguide 2. The purpose is to calculate for a given mode (n_1, m_1), the

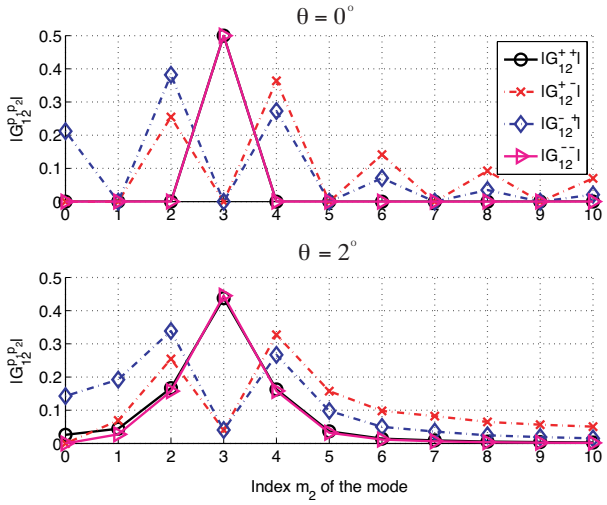

Figure 6. Functions $\{|G_{12}^{p_1p_2}|\}$ expressed from Eq. (C12) versus the index of the mode m_2 and the tilt angle $\theta_{12} = \{0, 2\}^\circ$. $a_1 = b_1 = 8\lambda_0$, $n = 2$, and $m_1 = 3$.

number of the modes m_2 ($n_2 = n_1$) which contributes to the scattering. From Eqs. (21)–(24), the elements of the matrix $\bar{\boldsymbol{\mathcal{T}}}_{ij}$ ($i = \{1, 2\}$ and $j = \{1, 2\}$) depend on the function $G_{12}^{p_1p_2}$ ($(p_1, p_2) = (+1, +1)$, $(p_1, p_2) = (-1, +1)$, $(p_1, p_2) = (+1, -1)$ and $(p_1, p_2) = (-1, -1)$) defined from Eq. (C12).

Figure 6 shows the moduli of $\{G_{12}^{p_1p_2}\}$ versus the index of the mode m_2 and the tilt angle $\theta_{12} = \{0, 2\}^\circ$, with $a_1 = b_1 = 8\lambda_0$, $n = 2$, and $m_1 = 3$. For $\theta_{12} = 0$, the functions $\{|G_{12}^{++}|, |G_{12}^{--}|\}$ contribute only for $m_2 = m_1$, which is consistent with Eq. (26). Moreover from Eq. (26), the functions $\{|G_{12}^{+-}|, |G_{12}^{-+}|\}$ vanish if the integer m_1+m_2 is odd, which is equivalent to have an even value for m_2 since $m_1 = 3$. For $\theta_{12} = 2^\circ$, the maxima of $\{|G_{12}^{++}|, |G_{12}^{--}|\}$ decreases weakly and the width of the diagrams increases, which means that the adjacent modes to m_1 have an influence on the scattering.

Figure 7 shows the moduli of the elements of the reflection matrix $\bar{\boldsymbol{\mathcal{R}}}_{is}$, given by Eq. (31), versus the index of the mode m_2 and the tilt angle $\theta_{12} = \{0, 2\}^\circ$, with $a_1 = b_1 = 8\lambda_0$, $n = 2$, and $m_1 = 3$. It is clearly observed that only few adjacent modes to $m_1 = 3$ contribute to the scattering, which is consistent with the observations of Fig. 6. Moreover, for $\theta_{12} = 0$, only the mode $m_2 = m_1$ exists for R_{is}^{hh} and R_{is}^{ee}, and $R_{is}^{\mathrm{he}} = R_{is}^{\mathrm{eh}} = 0$.

Thus, a means to calculate the range $m_2 \in [m_{2,\min}; m_{2,\max}]$ of

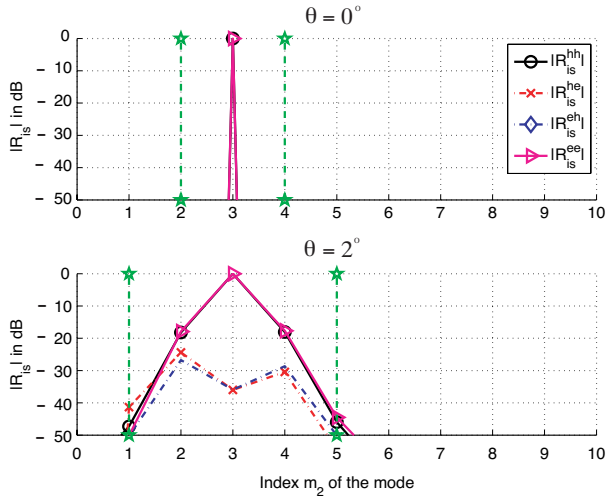

Figure 7. Moduli of the elements of the reflection matrix $\bar{\boldsymbol{\mathcal{R}}}_{is}$ given by Eq. (31) versus the index of the mode m_2 and the tilt angle $\theta_{12} = \{0, 2\}^\circ$. $a_1 = b_1 = 8\lambda_0$, $n = 2$, and $m_1 = 3$.

the modes contributing in the waveguide 2, is to study the function $G_{12}^{p_1 p_2}$ given by Eq. (C12). It is defined as the sum of four functions $e^{j\xi_{12}^{s_1 s_2}}\mathrm{sinc}(\xi_{12}^{s_1 s_2})$, where $\xi_{12}^{s_1 s_2} = \frac{1}{2} b \beta_{12}^{s_1 s_2} \cos\theta_2$, in which $\beta_{12}^{s_1 s_2} = s_1 k_{m_1} + s_2 k_{m_2} + \tan\theta_2(\beta_1 + \beta_2)$. Thus, chosen an integer p_2 such as $\xi_{12}^{s_1 s_2}/\pi = p_2$, it is possible to find a range of $m_2 \in [m_{2,\min}; m_{2,\max}]$, in which the functions $\{G_{12}^{p_1 p_2}\}$ contribute significantly. For small values of the tilt angle θ_{12}, it can be shown

$$m_{2,\min} = m_1 - \lfloor \Delta m_2 \rfloor_+ \quad m_{2,\max} = m_1 + \lfloor \Delta m_2 \rfloor_+ , \tag{46}$$

with

$$\Delta m_2 = \frac{\theta_{12}}{2}\left[2\gamma_1 + \sqrt{\gamma_1^2 + 4p_2\,(m_1 + p_2)}\right] + p_2 \quad \gamma_1 = \frac{\beta_1 b}{\pi}, \tag{47}$$

where $\lfloor x \rfloor_+$ rounds the variable x to the nearest integer towards infinity. Unlike Eq. (44), the function $\lfloor x \rfloor_+$ is used to avoid $\Delta m_2 = 0$. For $p_2 = 1$, in Fig. 7, the vertical dashed lines indicate the values of $m_{2,\min}$ and $m_{2,\max}$. It can be observed for $m_2 \notin [m_{2,\max}; m_{2,\min}]$ that the moduli of the elements of the matrix $\bar{\boldsymbol{\mathcal{R}}}_{is}$ do not contribute and $\lfloor \Delta m_2 \rfloor_+ = 2$. Further simulations, not shown here, confirm that $p_2 = 1$ is a good choice.

4.3. Simulations for One Bend

Figures 8 and 9 present the monostatic RCS $\sigma_{\theta\theta}$ and $\sigma_{\phi\phi}$ in dB m^2 obtained by FEKO, respectively, versus θ and $\theta_{12} = \{0, 1, 2, 5\}^\circ$. $a_1 = b_1 = 8\lambda_0$, $L_1 = 5\lambda_0$, $L_2 = 4\lambda_0$, $\phi = 0$ and the cavity is presented in Fig. 1. As the tilt angle θ_{12} increases, the RCSs decrease and this diminution is more significative for the $\phi\phi$ component.

Figures 10–11 present the same variations as in Fig. 8 but $\theta_{12} = 2^\circ$ and the results of our approach ("Modal") and IPO method ("IPO") are added. As we can see, our approach overpredicts slightly the RCSs,

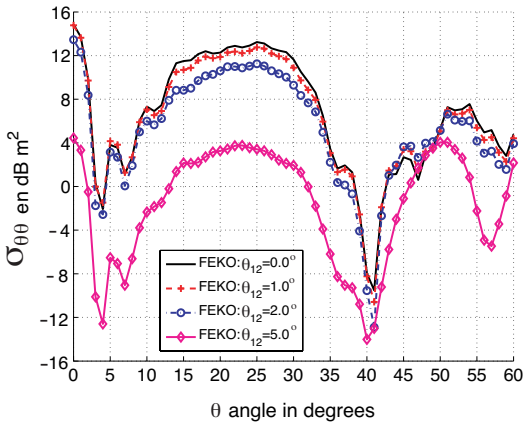

Figure 8. Monostatic RCS $\sigma_{\theta\theta}$ in dB m^2 versus θ and $\theta_{12} = \{0, 1, 2, 5\}^\circ$. $a_1 = b_1 = 8\lambda_0$, $L_1 = 5\lambda_0$, $L_2 = 4\lambda_0$, and $\phi = 0$.

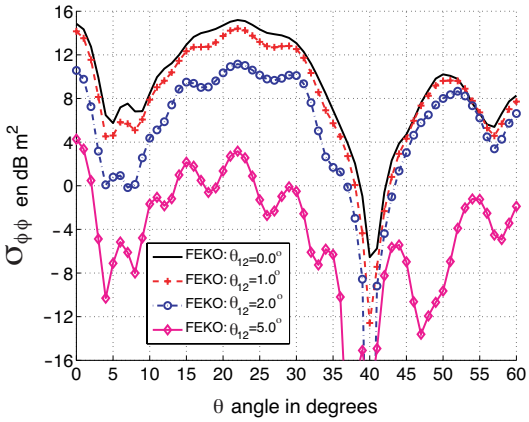

Figure 9. Same as in Fig. 8 but for $\sigma_{\phi\phi}$.

but allows to correct the difference of level observed in Figs. 8–9 due to the bend.

For $a_1 = b_1 = 6\lambda_0$, numerical results not shown here, leads to the same comment. Similar to our approach, the IPO method neglects the edge diffraction, and thus, the difference observed in Figs. 10–11 can not be attributed to this phenomenon since the IPO results match well with the FEKO ones. For $\theta_{12} = 5°$, comparisons (not reported here) between IPO, MLFMM, and Modal approaches, show disagreement between the Modal and MLFMM results, whereas the

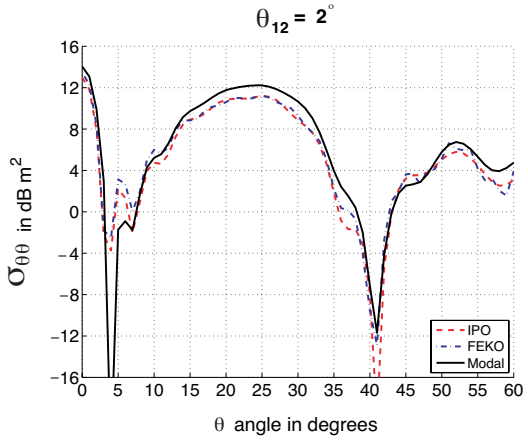

Figure 10. Same as in Fig. 8 but $\theta_{12} = 2°$ and the results of our approach are added.

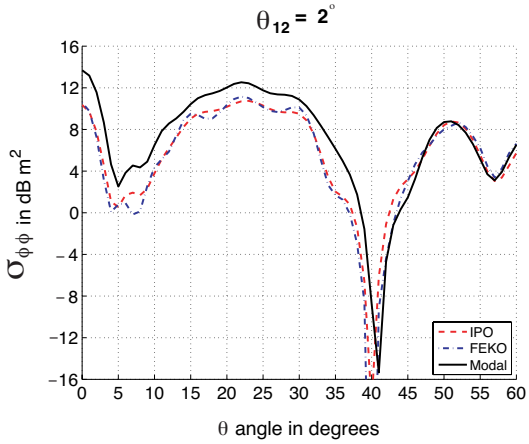

Figure 11. Same as in Fig. 10 but for $\sigma_{\phi\phi}$.

IPO ones coincide with the MLFMM ones.

Thus, this disagreement comes from the fact that when the boundary conditions are applied at the bend (surface Σ_{12} in Fig. 1), it was assumed that the electromagnetic modal fields at $z_1 = L_1$ are the same as $z_1 = L_1 + l_1$. In electromagnetic point of view, this means that the length l_1 should not to exceed some fraction of the wavelength λ_1 of the waveguide 1 (typically, $l_1 \leq 0.1 - 0.2\lambda_1$) defined as

$$\lambda_1^2 = \frac{\lambda_0^2}{1 - \left(\frac{n_1\lambda_0}{2a_1}\right)^2 - \left(\frac{m_1\lambda_0}{2b_1}\right)^2}. \tag{48}$$

This constraint also holds for the length l_2. If $a_1 \gg \lambda_0$ and $b_1 \gg \lambda_0$ then $\lambda_1 \approx \lambda_0$. From Fig. 5, since $n_{1,\min}$ and $m_{1,\min}$ increase with θ, λ_1 increases and $\lambda_1 > \lambda_0$. As a conclusion, $l_1 = l_2 \ll \lambda_0$.

From Fig. 1, $l_1 = l_2 = b\tan(\theta_{12}/2)$, and since $a_1 \gg \lambda_0$ and $b_1 \gg \lambda_0$ to be consistent with the Kirchhoff approximation, θ_{12} must be small. This implies $l_1 = l_2 \approx 0.00873b\theta_{12}$ with θ_{12} in degrees. Thus, if $l_1 \leq 0.1\lambda_0$, then with $b_1 = 8\lambda_0$, $\theta_{12} \leq 1.43^{\text{o}}$. If $\theta_{12} = 2^{\text{o}}$, then $l_1 = 0.14\lambda_0$. Further simulations with $\theta_{12} = \{1, 2.5, 3\}^{\text{o}}$, $a_1 = b_1 = \{6, 8\}\lambda_0$ (not presented here) show that $l_1 \leq 0.15\lambda_0$.

Figures 12–13 present the same results as in Figs. 10–11, but the length of the waveguide 2 is $L_2 = \lambda_0$. As expected, the length L_2 has not impact on the precision of the Modal method.

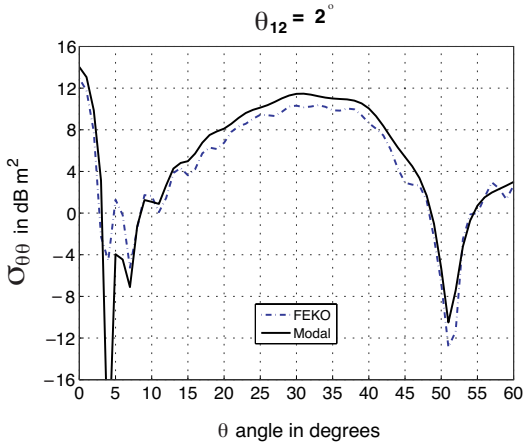

Figure 12. Same as in Fig. 10 but the length of the waveguide 2 is $L_2 = \lambda_0$.

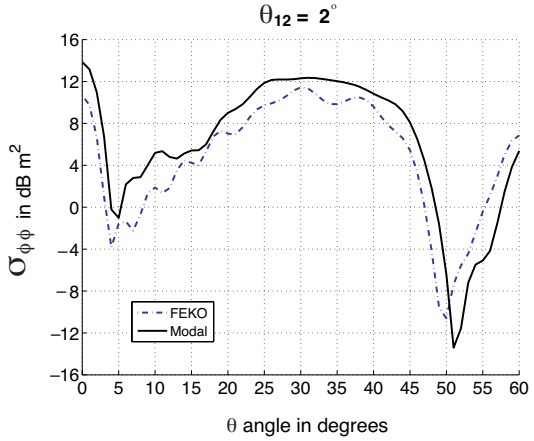

Figure 13. Same as in Fig. 12 but for $\sigma_{\phi\phi}$.

As a general conclusion of this subsection, the modal analysis combined with the Kirchhoff approximation is valid for small lengths l_1, typically $l_1 \leq 0.15\lambda_0$, and since the aperture must be large, the tilt angle θ_{12} can not exceed 2 degrees.

4.4. Simulations for Three Bends

As presented in Fig. 2, this subsection is devoted to the calculation of the monostatic RCS of connected rectangular waveguides of same cross section and uniforms along the $\hat{\mathbf{z}}$ direction stuffed by a perfectly-conducting termination. The angle θ_{ij} of the bend number $i \in [1; N_{\text{wg}} - 1]$ $(j = i + 1)$ is the tilt angle defined along the constant direction $\hat{\mathbf{z}}_1$, and $\theta_{r,ij}$ is defined along the direction $\hat{\mathbf{z}}_i$ with $\theta_{r,12} = \theta_{12}$.

Figures 14 and 15 present the monostatic RCS $\sigma_{\theta\theta}$ and $\sigma_{\phi\phi}$ in $\text{dB}\,\text{m}^2$, respectively, versus θ. $a_1 = b_1 = 8\lambda_0$, $L_1 = 5\lambda_0$, $L_1 = L_2 = L_3 = \lambda_0$, $\theta_{r,ij} = \{0.5, 1, 2, 3\}^{\text{o}}$ and $\phi = 0$.

For scattering angles θ smaller 45^{o}, similar behaviours as those observed in Figs. 8–9 are found, whereas for $\theta > 45^{\text{o}}$, the impact of the bends on the RCSs is less important because the results becomes similar.

Figures 16–17 present the monostatic RCS $\sigma_{\theta\theta}$ and $\sigma_{\phi\phi}$ in $\text{dB}\,\text{m}^2$, respectively, versus θ. $a_1 = b_1 = 8\lambda_0$, $L_1 = 5\lambda_0$, $L_1 = L_2 = L_3 = \lambda_0$, $\theta_{r,ij} = 2^{\circ}$ and $\phi = 0$. In the legend, "Modal non" means that the non-diagonal elements of the matrix $\bar{\boldsymbol{\mathcal{R}}}_{is}$ in Eq. (42) are assumed to be zero ($R_{is}^{\text{he}} = R_{is}^{\text{eh}} = 0$, non depolarizing effect on each bend). As we can see, a good agreement is obtained with the FEKO results, and the

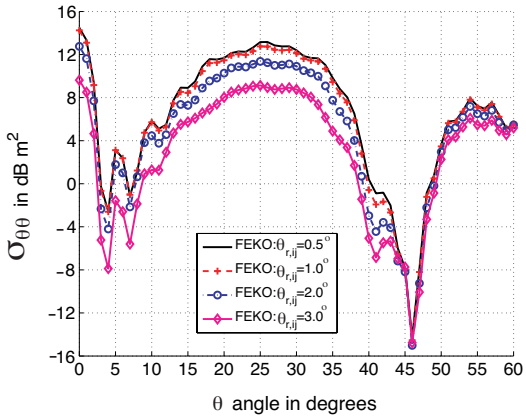

Figure 14. Monostatic RCS $\sigma_{\theta\theta}$ in $\mathrm{dB\,m^2}$ versus θ and $\theta_{r,ij} = \{0.5, 1, 2, 3\}^\circ$. $a_1 = b_1 = 8\lambda_0$, $L_1 = 5\lambda_0$, $L_1 = L_2 = L_3 = \lambda_0$, and $\phi = 0$.

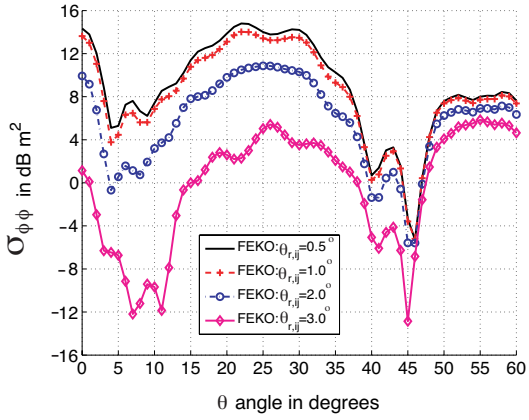

Figure 15. Same as in Fig. 14 but for $\sigma_{\phi\phi}$.

depolarizing effect on each bend must be taken into account for the $\theta\theta$ component, whereas for the $\phi\phi$, it can be neglected.

Simulations done for $\theta_{r,ij} = 3^\circ$ (not shown here) show that our approach is not valid to predict the monostatic RCS. It is consistent with the conclusion of the previous subsection, because the length l_i for each waveguide i does not satisfy the criterion $l_i \leq 0.15\lambda_0$.

Figures 18–19 ($N_{\mathrm{wg}} = 2$ with $\theta_{12} = 2^\circ$ and $L_2 = 4\lambda_0$) present the same variations as in Figs. 10–11, respectively, but the results obtained

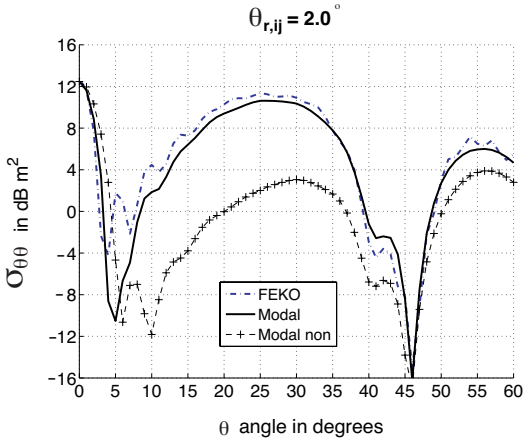

Figure 16. Same as in Fig. 14 but $\theta_{r,ij} = 2^{\text{o}}$ and the results of our approach are added.

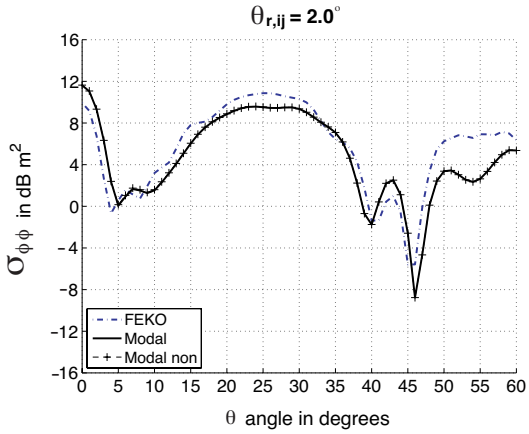

Figure 17. Same as in Fig. 16 but for $\sigma_{\phi\phi}$.

from $N_{\text{wg}} = 4$ ($\theta_{12} = \theta_{23} = \theta_{34} = 1^{\text{o}}$ and $L_2 = L_3 = L_4 = 1.3335\lambda_0$) are added. As we can see, when the tilt angle θ_{ij} decreases (from 2 to 1 degree), the results decreases slightly but do not improve significantly the agreement with the FEKO results. Thus, it is more convenient to use $N_{\text{wg}} = 2$ (3 sums), because the computing time is smaller comparatively to that obtained with $N_{\text{wg}} = 4$ (5 sums).

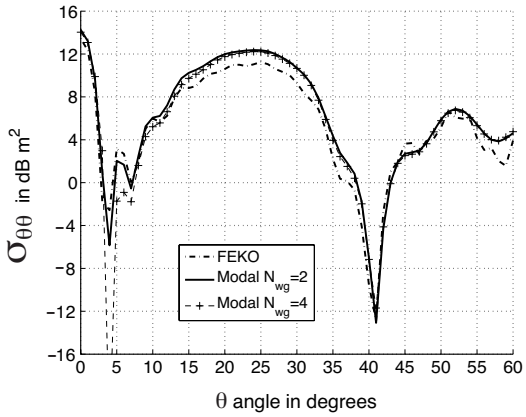

Figure 18. Same as in Fig. 10 ($N_{\text{wg}} = 2$ with $\theta_{12} = 2^\circ$ and $L_2 = 4\lambda_0$) but the results obtained from $N_{\text{wg}} = 4$ ($\theta_{12} = \theta_{23} = \theta_{34} = 1^\circ$ and $L_2 = L_3 = L_4 = 1.3335\lambda_0$) are added.

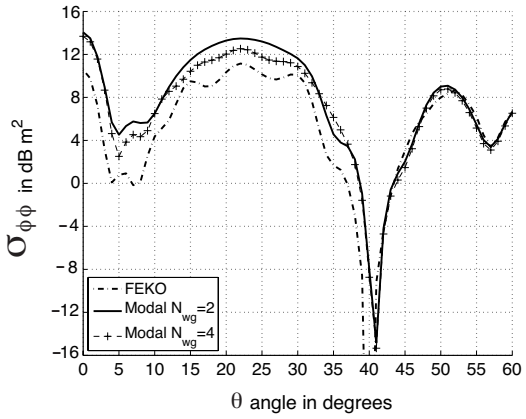

Figure 19. Same as in Fig. 18 but for $\sigma_{\phi\phi}$.

5. CONCLUSION

By modeling a cavity as a succession of connected bent waveguides of the same cross section and stuffed by a perfectly-conducting termination, a method based on a modal analysis combined with the Kirchhoff approximation is presented in this paper to predict the monostatic RCS of a cavity in high-frequency.

From this way, closed-form expressions of the transmission matrix

at each discontinuity can be obtained, which avoids to invert a matrix if rigorous boundary conditions are applied. In addition, this approach helps us to better understand the physical mechanisms, like the depolarizing effect and the mode conversion, which occur on a bend. Indeed, for a given mode (m_i, n_i) in the waveguide i ($i \in [1; N_{\text{wg}} - 1]$), the mode indexes (n_j, m_j) ($j = i + 1$) of the following connected waveguide j, which contributes to the scattering, are $n_j = n_i$ and $m_j \in [m_i - \Delta m_j; m_i + \Delta m_j]$ with Δm_j typically equals 2.

In addition with $\phi = 0°$, for the $\phi\phi$ component of the RCS, the depolarizing effect at each bend can be neglected, whereas for the $\theta\theta$ component, it must be accounted for. Comparing our method with the Iterated Physical Optics (IPO) method and the Multi-Level Fast Multipole Method (MLFMM, generated by using the commercial software FEKO), it is shown that the model is valid if the dimensions $\{l_i\}$ (see Fig. 1) do not exceed $0.15\lambda_0$, where λ_0 is the electromagnetic wavelength in the vacuum. Since, the cavity aperture must be large comparatively to λ_0, this constraint implies that each bend tilt angle can not exceed approximatively 2 degrees.

To overcome this drawback, instead of using for the second bent waveguide, the eigen functions of a waveguide uniform with respect to $\hat{\mathbf{z}}$ direction, the eigen functions of a curved waveguide along the $\hat{\mathbf{z}}$ direction [24] can be used. The advantage of this way is that the curvature effect of the waveguide is included in the eigen functions, whereas its main drawback, is that the mathematical expressions of the eigen functions are more complicated. The equations established in this paper are valid for any eigen functions. From this way, a more complex non-uniform cavity with respect to $\hat{\mathbf{z}}$ direction, like COBRA cavity, can be treated. The cavity is then truncated of elementary cavities, for which the eigen functions can be derived from a modal analysis, and the junctions between them are made with the Kirchhoff approximation and the reciprocity theorem.

APPENDIX A. DERIVATION OF A_1^+ FOR ANY CANONICAL WAVEGUIDE

For a plane wave, the electric field in a spherical coordinates $(\hat{\mathbf{k}}_i, \hat{\boldsymbol{\theta}}_i, \hat{\boldsymbol{\phi}}_i)$ can be expressed as $\mathbf{E}_i = (E_{i\theta}\hat{\boldsymbol{\theta}}_i + E_{i\phi}\hat{\boldsymbol{\phi}}_i)e^{jk_0\hat{\mathbf{k}}_i\cdot\mathbf{R}}$, in which $\mathbf{R}$ is a vector position defined in Cartesian coordinates as $\mathbf{R} = x\hat{\mathbf{x}} + y\hat{\mathbf{y}} + z\hat{\mathbf{z}}$. $k_0 = 2\pi/\lambda_0$ stands for the wavenumber in the vacuum. From the Kirchhoff approximation, the surface currents on Σ_1 are $\mathbf{J}_{s0}^+ = \hat{\mathbf{n}}_1 \wedge \mathbf{H}_i = \hat{\mathbf{z}}_1 \wedge \mathbf{H}_i$ (electric) and $\mathbf{M}_{s0}^+ = -\hat{\mathbf{n}}_1 \wedge \mathbf{E}_i = -\hat{\mathbf{z}}_1 \wedge \mathbf{E}_i$ (magnetic). Thus in Eq. (3), we have $(\mathbf{e}_{\text{T},1}^{\pm} + \mathbf{e}_{z,1}^{\pm}) \cdot \mathbf{J}_{s0}^+ = \mathbf{e}_{\text{T},1}^{\pm} \cdot (\hat{\mathbf{z}}_1 \wedge \mathbf{H}_i)$ and $(\mathbf{h}_{\text{T},1}^{\pm} + \mathbf{h}_{z,1}^{\pm}) \cdot \mathbf{M}_{s0}^+ =$

$-\mathbf{h}^{\pm}_{\mathrm{T},1} \cdot (\hat{\mathbf{z}}_1 \wedge \mathbf{E}_i)$.

In addition, since $\mathbf{H}_i = Y_0 \hat{\mathbf{k}}_i \wedge \mathbf{E}_i$ (Y_0 is the admittance of vacuum), the scalar product $\mathbf{e}^{\pm}_{\mathrm{T},1} \cdot (\hat{\mathbf{z}}_1 \wedge \mathbf{H}_i) = Y_0 \mathbf{e}^{\pm}_{\mathrm{T},1} \cdot [\hat{\mathbf{z}}_1 \wedge (\hat{\mathbf{k}}_i \wedge \mathbf{E}_i)] = Y_0[(\mathbf{e}^{\pm}_{\mathrm{T},1} \cdot \hat{\mathbf{k}}_i)(\hat{\mathbf{z}}_1 \cdot \mathbf{E}_i) - (\mathbf{e}^{\pm}_{\mathrm{T},1} \cdot \mathbf{E}_i)(\hat{\mathbf{z}}_1 \cdot \hat{\mathbf{k}}_i)]$.

The basis $(\hat{\mathbf{k}}_i, \hat{\boldsymbol{\theta}}_i, \hat{\boldsymbol{\phi}}_i)$ is related to the basis $(\hat{\mathbf{x}}_1, \hat{\mathbf{y}}_1, \hat{\mathbf{z}}_1)$ by a rotation matrix $\bar{\mathbf{R}}_3$

$$\left[\hat{\mathbf{k}}_i \ \hat{\boldsymbol{\theta}}_i \ \hat{\boldsymbol{\phi}}_i\right]^{\mathrm{T}} = \bar{\mathbf{R}}_3 \left[\hat{\mathbf{x}}_1 \ \hat{\mathbf{y}}_1 \ \hat{\mathbf{z}}_1\right]^{\mathrm{T}} \tag{A1}$$

with

$$\bar{\mathbf{R}}_3 = \begin{bmatrix} \sin\theta_i \cos\phi_i & \sin\theta_i \sin\phi_i & \cos\theta_i \\ \cos\theta_i \cos\phi_i & \cos\theta_i \sin\phi_i & -\sin\theta_i \\ -\sin\phi_i & \cos\phi_i & 0 \end{bmatrix} \quad \text{and} \quad \bar{\mathbf{R}}_3^{-1} = \bar{\mathbf{R}}_3^{\mathrm{T}}, \tag{A2}$$

where the superscript T stands for the transpose. Thus, we can show that the integrand of the numerator (3) is simplified as

$$\begin{cases} \mathbf{e}^{\pm}_{\mathrm{T},1} \cdot \hat{\mathbf{z}}_1 \wedge \mathbf{H}_i = Y_0 \Big[-E_{i\theta} \Big(e^{\pm}_{x,1} \cos\phi_i + e^{\pm}_{y,1} \sin\phi_i \Big) \\ \qquad\qquad + E_{i\phi} \cos\theta_i \Big(e^{\pm}_{x,1} \sin\phi_i - e^{\pm}_{y,1} \cos\phi_i \Big) \Big] e^{jk_0 \hat{\mathbf{k}}_i \cdot \mathbf{R}} \\ \mathbf{h}^{\pm}_{\mathrm{T},1} \cdot \hat{\mathbf{z}} \wedge \mathbf{E}_i = \Big[E_{i\theta} \cos\theta_i \Big(-h^{\pm}_{x,1} \sin\phi_i + h^{\pm}_{y,1} \cos\phi_i \Big) \\ \qquad\qquad - E_{i\phi} \Big(h^{\pm}_{x,1} \cos\phi_i + e^{\pm}_{y,1} \sin\phi_i \Big) \Big] e^{jk_0 \hat{\mathbf{k}}_i \cdot \mathbf{R}} \end{cases} . \tag{A3}$$

Thus

$$\mathbf{e}^{\pm}_{\mathrm{T},1} \cdot \hat{\mathbf{z}}_1 \wedge \mathbf{H}_i + \mathbf{h}^{\pm}_{\mathrm{T},1} \cdot \hat{\mathbf{z}} \wedge \mathbf{E}_i = -\frac{1}{k_0 \sin\theta_i} \left(E_{i\theta} \alpha_{\theta_i} + E_{i\phi} \alpha_{\phi_i} \right) e^{jk_0 \hat{\mathbf{k}}_i \cdot \mathbf{R}}, \tag{A4}$$

with

$$\begin{cases} \alpha_{\theta_i} = Y_0 \left(k_{ix} e^{\pm}_{x,1} + k_{iy} e^{\pm}_{y,1} \right) + \cos\theta_i \left(k_{iy} h^{\pm}_{x,1} - k_{ix} h^{\pm}_{y,1} \right) \\ \alpha_{\phi_i} = \left(k_{ix} h^{\pm}_{x,1} + k_{iy} h^{\pm}_{y,1} \right) + Y_0 \cos\theta_i \left(k_{ix} e^{\pm}_{y,1} - k_{iy} e^{\pm}_{x,1} \right) \end{cases} , \tag{A5}$$

and $e^{\pm}_{x,1} = \mathbf{e}^{\pm}_1 \cdot \hat{\mathbf{x}}_1$, $e^{\pm}_{y,1} = \mathbf{e}^{\pm}_1 \cdot \hat{\mathbf{y}}_1$, $h^{\pm}_{x,1} = \mathbf{h}^{\pm}_1 \cdot \hat{\mathbf{x}}_1$, $h^{\pm}_{y,1} = \mathbf{h}^{\pm}_1 \cdot \hat{\mathbf{y}}_1$, $k_{ix} = k_0 \sin\theta_i \cos\phi_i = \mathbf{k}_i \cdot \hat{\mathbf{x}}$ and $k_{iy} = k_0 \sin\theta_i \sin\phi_i = \mathbf{k}_i \cdot \hat{\mathbf{y}}$. The normalized components $\{e^{\pm}_{x,1}, e^{\pm}_{y,1}, h^{\pm}_{x,1}, h^{\pm}_{y,1}\}$ are given from Eqs. (1)

and (2) divided by k_0^2 in order to obtain dimensionless quantities. Thus reporting the above equations in Eq. (3), we have

$$\left\{ \begin{array}{l} A_1^{+,\mathrm{h}} = \frac{k_0 Y_0}{2\beta_1^{\mathrm{h}} P_1^{\mathrm{h}} \sin\theta_i} \left(E_{i\theta} \alpha_{\theta_i}^{\mathrm{h}} + E_{i\phi} \alpha_{\phi_i}^{\mathrm{h}} \right) \\ A_1^{+,\mathrm{e}} = \frac{k_0}{2\beta_1^{\mathrm{e}} P_1^{\mathrm{e}} \sin\theta_i} \left(E_{i\theta} \alpha_{\theta_i}^{\mathrm{e}} + E_{i\phi} \alpha_{\phi_i}^{\mathrm{e}} \right) \end{array} \right. , \tag{A6}$$

with

$$\left\{ \begin{array}{l} \alpha_{\theta_i}^{\mathrm{h}} = -j \left(k_{ix} G_y^{\mathrm{h}} - k_{iy} G_x^{\mathrm{h}} \right) \left(1 + \frac{\beta^{\mathrm{h}}}{k_0} \cos\theta_i \right) \\ \alpha_{\phi_i}^{\mathrm{h}} = j \left(k_{ix} G_x^{\mathrm{h}} + k_{iy} G_y^{\mathrm{h}} \right) \left(\frac{\beta^{\mathrm{h}}}{k_0} + \cos\theta_i \right) \\ \alpha_{\theta_i}^{\mathrm{e}} = j \left(k_{ix} G_x^{\mathrm{e}} + k_{iy} G_y^{\mathrm{e}} \right) \left(\frac{\beta^{\mathrm{e}}}{k_0} + \cos\theta_i \right) \\ \alpha_{\phi_i}^{\mathrm{e}} = j \left(k_{ix} G_y^{\mathrm{e}} - k_{iy} G_{e,x} \right) \left(1 + \frac{\beta^{\mathrm{e}}}{k_0} \cos\theta_i \right) \end{array} \right. \tag{A7}$$

in which

$$\left\{ \begin{array}{l} G_{x,y}^{\mathrm{h,e}} = \displaystyle\int_{\Sigma_1} e^{j(k_{ix}x + k_{iy}y)} \nabla_{x,y} \psi^{\mathrm{h,e}} d\Sigma \\ P_1^{\mathrm{h,e}} = \displaystyle\int_{\Sigma_1} \left[\left(\nabla_x \psi^{\mathrm{h,e}} \right)^2 + \left(\nabla_y \psi^{\mathrm{h,e}} \right)^2 \right] d\Sigma \end{array} \right. , \tag{A8}$$

with $\nabla_x = \frac{\partial}{\partial x}$, $\nabla_y = \frac{\partial}{\partial y}$.

For a rectangular waveguide, the eigen functions are expressed as

$$\left\{ \begin{array}{l} \psi^{\mathrm{h}}(x,y) = \cos\left(k_{n_1} x\right) \cos\left(k_{m_1} y\right) \\ \psi^{\mathrm{e}}(x,y) = \sin\left(k_{n_1} x\right) \sin\left(k_{m_1} y\right) \end{array} \right. , \tag{A9}$$

with $k_{n_1} = \frac{n_1 \pi}{a}$ and $k_{m_1} = \frac{m_1 \pi}{b}$. For the TE case, $n_1 + m_1 > 0$, whereas for the TM case, $n_1 > 0$ and $m_1 > 0$. Moreover, $\beta_1^{\mathrm{e}} = \beta_1^{\mathrm{h}} = \sqrt{k_0^2 - k_{n_1}^2 - k_{m_1}^2}$. Thus, Eq. (A8) becomes

$$\left\{ \begin{array}{l} G_x^{\mathrm{h}} = -k_{n_1} G_s(k_{ix}, a, n_1) G_c(k_{iy}, b, m_1) \\ G_y^{\mathrm{h}} = -k_{m_1} G_c(k_{ix}, a, n_1) G_s(k_{iy}, b, m_1) \\ G_x^{\mathrm{e}} = +k_{n_1} G_c(k_{ix}, a, n_1) G_s(k_{iy}, b, m_1) \\ G_y^{\mathrm{e}} = +k_{m_1} G_s(k_{ix}, a, n_1) G_c(k_{iy}, b, m_1) \end{array} \right. , \tag{A10}$$

$$P_1^{\mathrm{h,e}} = \frac{\varepsilon_{n_1}^{\mathrm{c}} \varepsilon_{m_1}^{\mathrm{c}} ab}{4} \left(k_{n_1}^2 + k_{m_1}^2 \right) , \tag{A11}$$

and $\varepsilon_{n_1}^{\mathrm{c}} = 2$ if $n_1 = 0$, 1 otherwise. Moreover

$$\begin{cases} G_c(k,a,n_1) = \displaystyle\int_0^a \cos(k_{n_1}x)\, e^{jkx} dx = jkG(k,a,n_1) \\ G_s(k,a,n_1) = \displaystyle\int_0^a \sin(k_{n_1}x)\, e^{jkx} dx = -k_{n_1} G(k,a,n_1) \end{cases}, \quad \text{(A12)}$$

with

$$G(k,a,n) = \frac{1-(-1)^n e^{jka}}{k^2 - \frac{n^2\pi^2}{a^2}}. \quad \text{(A13)}$$

Equation (A10) is then simplified as

$$\begin{cases} G_x^{\mathrm{h}} = +jk_{iy}G(k_{ix},a,n_1)G(k_{iy},b,m_1)k_{n_1}^2 \\ G_y^{\mathrm{h}} = +jk_{ix}G(k_{ix},a,n_1)G(k_{iy},b,m_1)k_{m_1}^2 \\ G_x^{\mathrm{e}} = -jk_{ix}G(k_{ix},a,n_1)G(k_{iy},b,m_1)k_{n_1}k_{m_1} \\ G_y^{\mathrm{e}} = -jk_{iy}G(k_{ix},a,n_1)G(k_{iy},b,m_1)k_{n_1}k_{m_1} \end{cases}. \quad \text{(A14)}$$

APPENDIX B. DERIVATION OF THE SCATTERED FIELD

In far-field, the components of the scattered field $(E_{s\theta}, E_{s\phi})$ in a spherical basis $(\hat{\mathbf{k}}_s, \hat{\boldsymbol{\theta}}_s, \hat{\boldsymbol{\phi}}_s)$ are expressed from the Huygens principle as [22]

$$\begin{cases} E_{s\theta} = \frac{jk_0 e^{-jk_0R_0}}{4\pi R_0} \hat{\boldsymbol{\theta}}_s \cdot \displaystyle\int_{\Sigma_1} \left[\hat{\mathbf{k}}_s \wedge \left(\mathbf{M}_{s0}^- - Z_0 \mathbf{J}_{s0}^- \wedge \hat{\mathbf{k}}_s\right) e^{jk_0 \hat{\mathbf{k}}_s \cdot \mathbf{R}}\right] d\Sigma \\ E_{s\phi} = \frac{jk_0 e^{-jk_0R_0}}{4\pi R_0} \hat{\boldsymbol{\phi}}_s \cdot \displaystyle\int_{\Sigma_1} \left[\hat{\mathbf{k}}_s \wedge \left(\mathbf{M}_{s0}^- - Z_0 \mathbf{J}_{s0}^- \wedge \hat{\mathbf{k}}_s\right) e^{jk_0 \hat{\mathbf{k}}_s \cdot \mathbf{R}}\right] d\Sigma \end{cases}, \quad \text{(B1)}$$

where the magnetic $\mathbf{J}_{s0}^-$ and electric $\mathbf{M}_{s0}^-$ currents are the unknown problem. As previously, their expressions can be obtained from the Kirchhoff approximation leading to $\mathbf{J}_{s0}^- = -\hat{\mathbf{z}}_1 \wedge \mathbf{H}_1^-$ and $\mathbf{M}_{s0}^- = \hat{\mathbf{z}}_1 \wedge \mathbf{E}_1^-$. The fields $(\mathbf{E}_1^-, \mathbf{H}_1^-)$ are the *reflected* fields onto the waveguide 1 expressed from Eqs. (1) and (2) with the subscript 1, and multiplying by the coefficients $\{A_1^{-,\mathrm{h}}, A_1^{-,\mathrm{e}}\}$ for each polarization.

Writing that $\mathbf{E}_1^- = E_{z,1}^- \hat{\mathbf{z}}_1 + \mathbf{E}_{\mathrm{T},1}^-$ et $\mathbf{H}_1^- = H_{z,1}^- \hat{\mathbf{z}}_1 + \mathbf{H}_{\mathrm{T},1}^-$, we show

$$\begin{aligned}\hat{\mathbf{k}}_s \wedge \left(\mathbf{M}_{s0}^- - Z_0 \mathbf{J}_{s0}^- \wedge \hat{\mathbf{k}}_s\right) \;=\; & \hat{\mathbf{z}}_1 \left(\hat{\mathbf{k}}_s \cdot \mathbf{E}_{\mathrm{T},1}^-\right) - \mathbf{E}_{\mathrm{T},1}^- \left(\hat{\mathbf{k}}_s \cdot \hat{\mathbf{z}}_1\right) \\ & + Z_0 \left[\left(\hat{\mathbf{z}}_1 \wedge \hat{\mathbf{k}}_s\right)\left(\hat{\mathbf{k}}_s \cdot \mathbf{H}_{\mathrm{T},1}^-\right)\right. \\ & \left. + \left(\hat{\mathbf{k}}_s \wedge \mathbf{H}_{\mathrm{T},1}^-\right)\left(\hat{\mathbf{k}}_s \cdot \hat{\mathbf{z}}_1\right)\right]. \qquad \text{(B2)}\end{aligned}$$

In FSA (Forward Scattering Alignment), the basis $(\hat{\mathbf{k}}_s, \hat{\boldsymbol{\theta}}_s, \hat{\boldsymbol{\phi}}_s)$ is expressed from the Cartesian basis $(\hat{\mathbf{x}}_1, \hat{\mathbf{y}}_1, \hat{\mathbf{z}}_1)$ from the rotation matrix defined by (A2), in which the incident angles (θ_i, ϕ_i) are substituted for the scattering (observation) angles (θ_s, ϕ_s). From Eqs. (B1) and (B2), the resulting equation is then

$$\left\{\begin{array}{l} E_{s\theta} = \frac{jk_0 e^{-jk_0 R_0}}{4\pi R_0} \displaystyle\int_{\Sigma_1} \Big[-\left(E_{x,1}^- \cos\phi_s + E_{y,1}^- \sin\phi_s\right) \\ \qquad + Z_0 \cos\theta_s \left(H_{x,1}^- \sin\phi_s - H_{y,1}^- \cos\phi_s\right)\Big] e^{jk_0 \hat{\mathbf{k}}_s \cdot \mathbf{R}} d\Sigma \\ E_{s\phi} = \frac{jk_0 e^{-jk_0 R_0}}{4\pi R_0} \displaystyle\int_{\Sigma_1} \Big[Z_0 \left(H_{x,1}^- \cos\phi_s + H_{y,1}^- \sin\phi_s\right) \\ \qquad + \cos\theta_s \left(E_{x,1}^- \sin\phi_s - E_{y,1}^- \cos\phi_s\right)\Big] e^{jk_0 \hat{\mathbf{k}}_s \cdot \mathbf{R}} d\Sigma \end{array}\right. . \qquad \text{(B3)}$$

The substitution of Eqs. (1) and (2) into (B3) leads to

$$\left\{\begin{array}{l} E_{s\theta} = \frac{je^{-jk_0 R_0} Z_0}{4\pi k_0 R_0 \sin\theta_s} \left(A_1^{-,\mathrm{h}} \alpha_{\theta_s}^{\mathrm{h}} + A_1^{-,\mathrm{e}} \alpha_{\theta_s}^{\mathrm{e}}\right) \\ E_{s\phi} = \frac{je^{-jk_0 R_0}}{4\pi k_0 R_0 \sin\theta_s} \left(A_1^{-,\mathrm{h}} \alpha_{\phi_s}^{\mathrm{h}} + A_1^{-,\mathrm{e}} \alpha_{\phi_s}^{\mathrm{e}}\right) \end{array}\right. , \qquad \text{(B4)}$$

with

$$\left\{\begin{array}{l} \alpha_{\theta_s}^{\mathrm{h}} = j\left(k_{sx} G_y^{\mathrm{h}} - k_{sy} G_x^{\mathrm{h}}\right)\left(1 + \frac{\beta^{\mathrm{h}}}{k_0} \cos\theta_s\right) \\ \alpha_{\phi_s}^{\mathrm{h}} = -j\left(k_{sx} G_x^{\mathrm{h}} + k_{sy} G_y^{\mathrm{h}}\right)\left(\frac{\beta^{\mathrm{h}}}{k_0} + \cos\theta_s\right) \\ \alpha_{\theta_s}^{\mathrm{e}} = j\left(k_{sx} G_x^{\mathrm{e}} + k_{sy} G_y^{\mathrm{e}}\right)\left(\frac{\beta^{\mathrm{e}}}{k_0} + \cos\theta_s\right) \\ \alpha_{\phi_s}^{\mathrm{e}} = j\left(k_{sx} G_y^{\mathrm{e}} - k_{sy} G_x^{\mathrm{e}}\right)\left(1 + \frac{\beta^{\mathrm{e}}}{k_0} \cos\theta_s\right) \end{array}\right. , \qquad \text{(B5)}$$

and $k_{sx} = k_0 \sin\theta_s \cos\phi_s = \mathbf{k}_s \cdot \hat{\mathbf{x}}$ and $k_{sy} = k_0 \sin\theta_s \sin\phi_s = \mathbf{k}_s \cdot \hat{\mathbf{y}}$. In addition, the functions $\{G_{x,y}^{\mathrm{h,e}}\}$ are expressed from (A8).

APPENDIX C. INTEGRATIONS OVER X_2 AND Y_2

The derivation of A_2^+ expressed from (8) needs the calculation of the integrations over x_2 and y_2. For a rectangular waveguide, the eigen functions are given by (A9). Thus

$$\left.\begin{array}{l} \nabla_x\psi^{\mathrm{e}}\big|_1\ \nabla_y\psi^{\mathrm{h}}\big|_2 = -k_{n_1}k_{m_2} \\ \nabla_x\psi^{\mathrm{e}}\big|_1\ \nabla_x\psi^{\mathrm{e}}\big|_2 = k_{n_1}k_{n_2} \\ \nabla_y\psi^{\mathrm{h}}\big|_1\ \nabla_y\psi^{\mathrm{h}}\big|_2 = k_{m_1}k_{m_2} \\ \nabla_y\psi^{\mathrm{h}}\big|_1\ \nabla_x\psi^{\mathrm{e}}\big|_2 = -k_{m_1}k_{n_2} \end{array}\right\} c_{n_1}c_{n_2}s_{m_1}s_{m_2}, \tag{C1}$$

$$\left.\begin{array}{l} \nabla_y\psi^{\mathrm{e}}\big|_1\ \nabla_x\psi^{\mathrm{h}}\big|_2 = -k_{m_1}k_{n_2} \\ \nabla_y\psi^{\mathrm{e}}\big|_1\ \nabla_y\psi^{\mathrm{e}}\big|_2 = k_{m_1}k_{m_2} \\ \nabla_x\psi^{\mathrm{h}}\big|_1\ \nabla_x\psi^{\mathrm{h}}\big|_2 = k_{n_1}k_{n_2} \\ \nabla_x\psi^{\mathrm{h}}\big|_1\ \nabla_y\psi^{\mathrm{e}}\big|_2 = -k_{n_1}k_{m_2} \end{array}\right\} s_{n_1}s_{n_2}c_{m_1}c_{m_2}, \tag{C2}$$

$$\left.\begin{array}{l} \nabla_x\psi^{\mathrm{e}}\big|_1\ \psi^{\mathrm{h}}\big|_2 = k_{n_1}s_{m_1}c_{m_2} \\ \psi^{\mathrm{h}}\big|_1\ \nabla_y\psi^{\mathrm{h}}\big|_2 = -k_{m_2}c_{m_1}s_{m_2} \\ \psi^{\mathrm{h}}\big|_1\ \nabla_x\psi^{\mathrm{e}}\big|_2 = k_{n_2}c_{m_1}s_{m_2} \\ \nabla_y\psi^{\mathrm{h}}\big|_1\ \psi^{\mathrm{h}}\big|_2 = -k_{m_1}s_{m_1}c_{m_2} \end{array}\right\} c_{n_1}c_{n_2}, \tag{C3}$$

and

$$\left.\begin{array}{l} \psi^{\mathrm{e}}\big|_1\ \nabla_x\psi^{\mathrm{h}}\big|_2 = -k_{n_2}s_{m_1}c_{m_2} \\ \psi^{\mathrm{e}}\big|_1\ \nabla_y\psi^{\mathrm{e}}\big|_2 = k_{m_2}s_{m_1}c_{m_2} \\ \nabla_y\psi^{\mathrm{e}}\big|_1\ \psi^{\mathrm{e}}\big|_2 = k_{m_1}c_{m_1}s_{m_2} \\ \nabla_x\psi^{\mathrm{h}}\big|_1\ \psi^{\mathrm{e}}\big|_2 = -k_{n_1}c_{m_1}s_{m_2} \end{array}\right\} s_{n_1}s_{n_2}, \tag{C4}$$

with $c_{n_i} = \cos(k_{n_i}x_i)$, $c_{m_i} = \cos(k_{m_i}y_i)$, $s_{n_i} = \sin(k_{n_i}x_i)$ and $s_{m_i} = \sin(k_{m_i}y_i)$. The above equations depend on $c_{n_1}c_{n_2} = \cos(k_{n_1}x_2)\cos(k_{n_2}x_2)$ and $s_{n_1}s_{n_2} = \sin(k_{n_1}x_2)\sin(k_{n_2}x_2)$, as functions of x_1 and x_2. Since $x_2 = x_1$, the integration over $x_2 \in [0; a]$ yields

$$\left.\begin{array}{l} \displaystyle\int_0^a s_{n_1}s_{n_2}dx_2 \\ \displaystyle\int_0^a c_{n_1}c_{n_2}dx_2 \end{array}\right\} = \frac{a}{2}\delta_{n_1,n_2}\left\{\begin{array}{l} \varepsilon_{n_1}^{\mathrm{s}} \\ \varepsilon_{n_1}^{\mathrm{c}} \end{array}\right. , \tag{C5}$$

with $\delta_{n_1,n_2} = 1$ if $n_1 = n_2$, 0 otherwise, $\varepsilon_{n_1}^{\mathrm{c}} = 2$ if $n_1 = 0$, 1 otherwise, and $\varepsilon_{n_1}^{\mathrm{s}} = 0$ if $n_1 = 0$, 1 otherwise. The Kronecker symbol δ_{n_1,n_2} shows

that a mode n_1 is not degenerated into several modes in the waveguide 2, because the waveguide 2 undergoes only a rotation with respect to the axial direction $\hat{\mathbf{x}}_2 = \hat{\mathbf{x}}_1$. The terms $\{\varepsilon_{n_1}^{\mathrm{c}}, \varepsilon_{n_1}^{\mathrm{s}}\}$ are different of the unity only for $n_1 = 0$. For the TM case, the mode $n = 0$ with $\forall\ m \geq 0$ is excluded, and $\{\varepsilon_{n_1}^{\mathrm{c}}, \varepsilon_{n_1}^{\mathrm{s}}\}$ can then be omitted. However, For the TE case with $m > 0$, the mode $n = 0$ exist and these terms must be then taken into account for $n_1 = n_2 = 0$ with $m_1 > 0$ and $m_2 > 0$. As a conclusion, the terms $\{\varepsilon_{n_1}^{\mathrm{c}}, \varepsilon_{n_1}^{\mathrm{s}}\}$ will be kept only for the TE case on the term $A_1^{+,\mathrm{h}}$.

To integrate over $y_2 \in [0; b\cos\theta_2]$, the following decompositions are used

$$\left\{\begin{array}{l} c_{m_1}c_{m_2} = \frac{1}{4}\displaystyle\sum_{s_1=\pm1}\sum_{s_2=\pm1} e^{j(s_1k_{m_1}y_1+s_2k_{m_2}y_2)} \\ s_{m_1}s_{m_2} = -\frac{1}{4}\displaystyle\sum_{s_1=\pm1}\sum_{s_2=\pm1} e^{j(s_1k_{m_1}y_1+s_2k_{m_2}y_2)}s_1s_2 \\ c_{m_1}s_{m_2} = \frac{1}{4j}\displaystyle\sum_{s_1=\pm1}\sum_{s_2=\pm1} e^{j(s_1k_{m_1}y_1+s_2k_{m_2}y_2)}s_2 \\ s_{m_1}c_{m_2} = \frac{1}{4j}\displaystyle\sum_{s_1=\pm1}\sum_{s_2=\pm1} e^{j(s_1k_{m_1}y_1+s_2k_{m_2}y_2)}s_1 \end{array}\right. . \tag{C6}$$

In Eqs. (14)–(16) and (17), the term $e^{j(\beta_2 z_2-\beta_1 z_1+s_1k_{m_1}y_1+s_2k_{m_2}y_2)}$ occurs ($\beta_{1,2}^{\mathrm{h}} = \beta_{1,2}^{\mathrm{e}} = \beta_{1,2}$). From Fig. 1, one has

$$\left\{\begin{array}{l} z_1 = +z_2\cos\theta_{12} - y_2\sin\theta_{12} - L_1 \\ y_1 = +z_2\sin\theta_{12} + y_2\cos\theta_{12} \\ z_2 = y_2\tan\theta_2 \end{array}\right. , \tag{C7}$$

which implies that

$$\begin{array}{rl} & \beta_2 z_2 - \beta_1 z_1 + s_1k_{m_1}y_1 + s_2k_{m_2}y_2 \\ = & \beta_1 L_1 + y_2\underbrace{\left[s_1k_{m_1} + s_2k_{m_2} + \tan\theta_2\left(\beta_1+\beta_2\right)\right]}_{\beta_{12}^{s_1s_2}}. \end{array} \tag{C8}$$

The integration over y_2 needs then to derive the following integral

$$\begin{array}{rl} & \displaystyle\int_0^{b\cos\theta_2} e^{j\beta_{12}^{s_1s_2}y_2}dy_2 = \frac{1}{j\beta_{12}^{s_1s_2}}\left(e^{jb\beta_{12}^{s_1s_2}\cos\theta_2} - 1\right) \\ = & \left(b\cos\theta_2\right)e^{\frac{jb\beta_{12}^{s_1s_2}\cos\theta_2}{2}}\mathrm{sinc}\left(\frac{b\beta_{12}^{s_1s_2}\cos\theta_2}{2}\right). \end{array} \tag{C9}$$

From the above equations and from Eqs. (14)–(16) and (17), the integration over x_2 and y_2 of the numerator of Eq. (8) leads for the TE case to

$$\begin{aligned}
&\frac{8e^{-j\beta_1 L_1}}{ab}\int_{\Sigma_{12}}\left[\left(\mathbf{e}^-_{\mathrm{T},2}+\mathbf{e}^-_{z,2}\right)\cdot\mathbf{J}^+_{s1}-\left(\mathbf{h}^-_{\mathrm{T},2}+\mathbf{h}^-_{z,2}\right)\cdot\mathbf{M}^+_{s1}\right]d\Sigma_{12}\\
&= k_0 Z_0 A_1^{+,\mathrm{h}}\times\Bigg[\cos\theta_2\left(\beta_1+\beta_2\right)\left(k_{n_1}k_{n_2}G_{12}^{++}\varepsilon_n^{\mathrm{s}}-k_{m_1}k_{m_2}G_{12}^{--}\varepsilon_n^{\mathrm{c}}\right)\\
&\quad+\sin\theta_2\left(k_{c_1}^2k_{m_2}G_{12}^{+-}+k_{c_2}^2k_{m_1}G_{12}^{-+}\right)\varepsilon_n^{\mathrm{c}}\Bigg]\\
&\quad+A_1^{+,\mathrm{e}}\Bigg[\cos\theta_2\left(k_0^2+\beta_1\beta_2\right)\left(k_{m_1}k_{n_2}G_{12}^{++}+k_{n_1}k_{m_2}G_{12}^{--}\right)\\
&\quad-\sin\theta_2\left(k_{c_1}^2k_{n_2}\beta_2+k_{c_2}^2k_{n_1}\beta_1\right)G_{12}^{-+}\Bigg],
\end{aligned}\tag{C10}$$

and for the TM case to

$$\begin{aligned}
&\frac{8e^{-j\beta_1 L_1}}{ab}\int_{\Sigma_{12}}\left[\left(\mathbf{e}^-_{\mathrm{T},2}+\mathbf{e}^-_{z,2}\right)\cdot\mathbf{J}^+_{s1}-\left(\mathbf{h}^-_{\mathrm{T},2}+\mathbf{h}^-_{z,2}\right)\cdot\mathbf{M}^+_{s1}\right]d\Sigma_{12}\\
&= k_0 Y_0 A_1^{+,\mathrm{e}}\times\Bigg[-\cos\theta_2\left(\beta_1+\beta_2\right)\left(k_{n_1}k_{n_2}G_{12}^{++}-k_{m_1}k_{m_2}G_{12}^{--}\right)\\
&\quad+\sin\theta_2\left(k_{c_1}^2k_{m_2}G_{12}^{-+}+k_{c_2}^2k_{m_1}G_{12}^{+-}\right)\Bigg]\\
&\quad-A_1^{+,\mathrm{h}}\Bigg[\cos\theta_2\left(k_0^2+\beta_1\beta_2\right)\left(k_{m_1}k_{n_2}G_{12}^{--}+k_{m_2}k_{n_1}G_{12}^{++}\right)\\
&\quad-\sin\theta_2\left(k_{c_1}^2k_{n_2}\beta_2+k_{c_2}^2k_{n_1}\beta_1\right)G_{12}^{+-}\Bigg],
\end{aligned}\tag{C11}$$

with

$$G_{12}^{p_1p_2}=\sum_{s_1=\pm1}\sum_{s_2=\pm1}e^{j\xi_{12}^{s_1s_2}}\mathrm{sinc}\left(\xi_{12}^{s_1s_2}\right)\begin{cases}+1 & \text{if}\quad p_1=p_2=+\\ s_1s_2 & \text{if}\quad p_1=p_2=-\\ s_2 & \text{if}\quad p_1=+,p_2=-\\ s_1 & \text{if}\quad p_1=-,p_2=+\end{cases}\tag{C12}$$

$$\xi_{12}^{s_1s_2}=\frac{b\beta_{12}^{s_1s_2}\cos\theta_2}{2},\tag{C13}$$

and $k_{n_1}=k_{n_2}=k_n=\frac{n\pi}{a}$ $(n=n_1=n_2)$, $k_{m_i}=\frac{m_i\pi}{b}$, $\beta_i=\sqrt{k_0^2-k_n^2-k_{m_i}^2}$ and $k_{c_i}^2=k_n^2+k_{m_i}^2$.

It should be noted that the factor $\frac{8}{a} = \frac{2}{a} \times 4$ in front of the integral comes from $\frac{a}{2}$ in Eq. (C5) and from $\frac{1}{4}$ in Eq. (C6), with the sign and the factor $\frac{1}{j}$ in (C6). Moreover, the term $\cos\theta_2$ in Eq. (C9) is absorbed by the term $\frac{1}{\cos\theta_2}$ in Eq. (19).

The denominator of Eq. (8) given by Eq. (19) requires also the derivation of the integrations over x_2 and y_2. Using the same way as previously, it can be shown that

$$\text{Eq. (19)} = \frac{ab\cos\theta_2}{8} \begin{cases} +k_{n_2}^2 G'^{++}_{12} - k_{m_2}^2 G'^{--}_{12} \varepsilon_{n_2}^{\mathrm{c}} & \text{TE case} \\ -k_{n_2}^2 G'^{--}_{12} + k_{m_2}^2 G'^{++}_{12} \varepsilon_{n_2}^{\mathrm{s}} & \text{TM case} \end{cases}, \tag{C14}$$

in which the function $G'^{p_1 p_2}_{12}$ is expressed from (C12), in which, $\beta_{12}^{s_1 s_2}$ is substituted for $\beta'^{s_1 s_2}_{12} = 2\beta_2 \tan\theta_2 + k_{m_2}(s_1 + s_2)$.

For the TM case, the mode $n = 0$ with $\forall\ m \geq 0$ is excluded, and the term $\varepsilon_{n_2}^{\mathrm{s}}$ in Eq. (C14) can then be omitted because $\varepsilon_{n_2}^{\mathrm{s}} = 1$ for $n_2 > 0$. On the other hand, for the TE case with $m > 0$, the mode $n = 0$ exist and the term $\varepsilon_{n_2}^{\mathrm{c}}$ in Eq. (C14) must be taken into account at $n_1 = n_2 = n = 0$ with $m_1 > 0$ and $m_2 > 0$. But, from Eq. (C10), the term after $A_1^{+,\mathrm{h}}$ between brackets and for $n = 0$ exhibits only $\varepsilon_n^{\mathrm{c}}$ terms, and they are then simplified by dividing by Eq. (C14). As a consequence, the terms $\varepsilon_n^{\mathrm{c}}$ and $\varepsilon_{n_2}^{\mathrm{s}}$ can be omitted in Eqs. (C10) and (C14). In conclusion, the substitution of Eqs. (10), (C11) and (C14) into Eq. (8) yields Eq. (20).

REFERENCES

1. Bopp, C. L. and C. M. Butler, "Analysis of transmission of a signal through a complex cylindrical/coaxial cavity by transmission line methods," *Progress In Electromagnetics Research*, Vol. 56, 33–51, 2006.
2. Nie, X. C., Y. B. Gan, N. Yuan, et al., "An efficient hybrid method for analysis of slot arrays enclosed by a large radome," *Journal of Electromagnetic Waves and Applications*, Vol. 20, 249–264, 2006.
3. Li, J. Y., L. W. Li, and Y. B. Gan, "Method of moments analysis of waveguide slot antennas using the EFIE," *Journal of Electromagnetic Waves and Applications*, Vol. 19, 1729–1748, 2005.
4. Anastassiu, H. T., "A review of electromagnetic scattering analysis for inlets, cavities and open ducts," *IEEE Ant. Prop. Magazine*, Vol. 45, No. 6, 27–40, 2003.

5. Ling, H., "RCS of waveguide cavities: A hybrid boundary integral/modal approach," *IEEE Trans. Ant. Prop.*, Vol. 38, No. 9, 1413–1420, 1990.
6. Ling, H., R. C. Chou, and S. W. Lee, "Shooting and bouncing rays: Calculating the RCS of an arbitrarily shaped cavity," *IEEE Trans. Ant. Prop.*, Vol. 37, No. 2, 194–205, 1989.
7. Pathak, P. H. and R. J. Burkholder, "Modal, ray, and beam techniques for analyzing the EM scattering by open-ended waveguide cavities," *IEEE Trans. Ant. Prop.*, Vol. 37, No. 5, 635–647, 1989.
8. Burkholder, R. J., R. C. Chou, and P. H. Pathak, "Two ray shooting methods for computing the EM scattering by large open-ended cavities," *Computer Physics Communications*, No. 68, 353–365, 1991.
9. Pathak, P. H. and R. J. Burkholder, "High-frequency electromagnetic scattering by open-ended waveguide cavities," *Radio Science*, Vol. 26, No. 1, 211–218, 1991.
10. Xu, L., J. Tian, and X. W. Shi, "A closed-form solution to analyze RCS of cavity with rectangular cross section," *Progress In Elecromagnetic Research*, PIER 80, 195–208, 2008.
11. Obelleiro, F., J. L. Rodriguez, and R. J. Burckholder, "An iterative physical optics approach for analyzing the electromagnetic scattering by large open-ended cavities," *IEEE Trans. Ant. Prop.*, Vol. 43, No. 4, 356–361, 1995.
12. Obelleiro, F., J. L. Rodriguez, and A. G. Pino, "A progressive physical optics (PPO) method for computing the electromagnetic scattering of large open-ended cavities," *Micro. Opt. Tech. Letters*, Vol. 14, No. 3, 1997.
13. Obelleiro, F., J. Campos-Niño, J. L. Rodriguez, and A. G. Pino, "A segmented approach for computing the electromagnetic scattering of large and deep cavities," *Progress In Elecromagnetics Research*, PIER 19, 129–145, 1998.
14. Hémon, R., P. Pouliguen, H. He, J. Saillard, and J. F. Damiens, "Computation of EM fields scattered by an open-ended cavity and by cavity under radome using the iterative phyisical optics," *Progress In Electromagnetics Research*, PIER 80, 77–105, 2008.
15. Lee, C. S. and S. W. Lee, "RCS of a coated circular waveguide terminated by a perfect conductor," *IEEE Trans. Ant. Prop.*, Vol. 35, No. 4, 391–398, 1987.
16. Altintas, A., P. H. Pathak, and M. C. Liang, "A selective modal scheme for the analysis of EM coupling into or radiation from large

open-ended waveguides," *IEEE Trans. Ant. Prop.*, Vol. 36, No. 1, 84–96, 1988.

17. Ling, H., S. W. Lee, and R. C. Chou, "High-frequency RCS of open cavities with rectangular and circular cross sections," *IEEE Trans. Ant. Prop.*, Vol. 37, No. 5, 648–654, 1989.
18. Ling, H. and H. Kim, "On the application of Kirchhoff's approximation to scattering from discontinuities in large waveguide ducts," *Microwave and Opt. Technology Letters*, Vol. 7, No. 4, 168–172, 1994.
19. Chan, K. K. and S. Wong, "Modal approach to RCS computation of electrically large inlets," *2002 IEEE International Symposium on Antennas and Propagation Digest*, Vol. 1, 114–117, San Antonio TX, June 16–21, 2002.
20. Anastassiu, H. T., J. L. Volakis, and D. C. Ross, "The mode matching technique for electromagnetic scattering by cylindrical waveguides with canonical terminations," *Journal of Electromagnetic Waves and Applications*, Vol. 9, No. 11/12, 1363–1391, 1995.
21. *FEKO User's Manual Suite 4.1*, EM Softw. Syst. Technopark-Stellenbosch, Africa, 2003.
22. Ishimaru, A., *Electromagnetic Wave Propagation, Radiation, and Scattering*, Prentice Hall, New Jersey, 1991.
23. Collin, R. E., *Field Theory of Guided Waves*, 2nd edition, IEEE Press, New York, 1991.
24. San Blas, A. A., B. Gimeno, V. E. Boria, H. Esteban, S. Cogollos, and A. Coves, "A rigorous and efficient full-wave analysis of uniform bends in rectangular waveguide under arbitrary incidence," *IEEE Trans. Micr. Techniques*, Vol. 51, No. 2, 397–405, 2003.